Published February 1, 2019

Original Research

Core Ideas

- Cosmic-ray neutron data are used to inversely estimate soil hydraulic properties.
- The forward neutron operator COSMIC is coupled with the vadose zone model HYDRUS-1D.
- Bayesian analyses confirm the information content of cosmic-ray neutron data.

On the Information Content of Cosmic-Ray Neutron Data in the Inverse Estimation of Soil Hydraulic Properties

Giuseppe Brunetti, Jiří Šimůnek, Heye Bogena, Roland Baatz, Johan Alexander Huisman, Helen Dahlke, and Harry Vereecken*

Observations of soil moisture content from remote sensing platforms can be used in conjunction with hydrological models to inversely estimate soil hydraulic properties (SHPs). In recent years, cosmic-ray neutron sensing (CRNS) has proven to be a reliable method for the estimation of area-average soil moisture at field scales. However, its use in the inverse estimation of the effective SHPs is largely unexplored. Thus, the main objective of this study was to assess the information content of aboveground fast-neutron counts to estimate SHPs using both a synthetic modeling study and actual experimental data from the Rollesbroich catchment in Germany. For this, the forward neutron operator COSMIC was externally coupled with the hydrological model HYDRUS-1D. The coupled model was combined with the Affine Invariant Ensemble Sampler to calculate the posterior distributions of effective soil hydraulic parameters as well as the model-predictive uncertainty for different synthetic and experimental scenarios. Measured water contents at different depths were used to assess estimated SHPs. The analysis of both synthetic and actual CRNS data from homogenous and heterogeneous soil profiles, respectively, led to confident estimations of the shape parameters α and n, while higher uncertainty was observed for the saturated hydraulic conductivity. Furthermore, results demonstrated that neutron data are less influenced by local sources of uncertainty compared with near-surface point measurements. The simultaneous use of CRNS and water content data further reduced the overall uncertainty, opening up new perspectives for the combination of CRNS with other remote sensing techniques for the inverse estimation of the effective SHPs.

Abbreviations: AIES, Affine Invariant Ensemble Sampler; CRNP, cosmic-ray neutron probe; CRNS, cosmic-ray neutron sensing; IAT, integrated autocorrelation time; LSM, land surface model; MCMC, Markov chain Monte Carlo; MCNPX, Monte Carlo N-Particle eXtended; PTF, pedotransfer function; SHPs, soil hydraulic properties; VGM, van Genuchten–Mualem.

G. Brunetti, Dep. of Land, Air and Water Resources, Univ. of California, Davis, CA 95616, and Institute of Hydraulics and Rural Water Management, Univ. of Natural Resources and Life Sciences (BOKU), Vienna, 1190, Austria; J. Šimůnek, Dep. of Environmental Sciences, Univ. of California, Riverside, CA 92521; H. Bogena, R. Baatz, J.A. Huisman, and H. Vereecken, Agrosphere Institute, Forschungszentrum Jülich GmbH, 52428 Jülich, Germany; H. Dahlke, Dep. of Land, Air and Water Resources, Univ. of California, Davis, CA 95616. *Corresponding author (h.vereecken@fz-juelich.de).

Received 26 June 2018.
Accepted 23 Sept. 2018.

Citation: Brunetti, G., J. Šimůnek, H. Bogena, R. Baatz, J.A. Huisman, H. Dahlke, and H. Vereecken. 2019. On the information content of cosmic-ray neutron data in the inverse estimation of soil hydraulic properties. Vadose Zone J. 18:180123. doi:10.2136/vzj2018.06.0123

Soil hydraulic properties (SHPs) define the relationship between volumetric water content (θ), pressure head (h), and hydraulic conductivity (K), thus regulating the movement of water in the soil and influencing the water–energy cycle at the land surface. In particular, the near-surface soil moisture has a profound influence on the partitioning of precipitation into surface runoff, evapotranspiration, and infiltration and thus on the surface energy balance. In this view, there is strong evidence that land surface processes play a key role in climate models (Pitman, 2003). An accurate description of hydrological processes at the land surface is thus of crucial importance.

Land surface models (LSMs) incorporating a mechanistic description of infiltration require precise estimation of large-scale SHPs. Typically, the measurement scale for the characterization of SHPs is on the order of 10 cm, with a sample spacing of 100 m or larger (Hopmans et al., 2002). In this perspective, the upscaling of point measurements is time consuming and introduces significant uncertainty into land surface hydrological modeling (Vereecken et al., 2007). To overcome this problem, pedotransfer functions (PTFs) are often used (Van Looy et al., 2017) to translate available soil textural information into SHPs. However, uncertainty in PTF inputs often propagates into the poor accuracy of SHPs (Deng et al., 2009).

A valid alternative is the inverse estimation of effective SHPs from transient data (Dane and Hruska, 1983; Kool and Parker, 1988; Šimůnek and van Genuchten, 1996; Iden and Durner, 2007; Ines and Mohanty, 2008; Vrugt et al., 2008a). For example, Gutmann and Small (2007) used the land surface model Noah (Ek et al., 2003) to compare the results obtained using inversely estimated and PTF-based SHPs. They found a significant reduction in errors between measured and simulated latent heat fluxes when inversely estimated SHPs were used. Moreover, the use of emerging global optimization algorithms and statistically rigorous methods based on Bayesian inference now allow obtaining both a reliable estimate of SHPs and a proper assessment of their uncertainty (e.g., Huisman et al., 2010; Scharnagl et al., 2011; Wöhling and Vrugt, 2011), which is directly related to the information content of the measured data used in the inverse estimation framework.

Traditionally, point measurements of pressure head and water content have been used for the inverse estimation of SHPs. However, during the last decade, soil moisture remote sensing techniques have gained popularity (Bogena et al., 2015; Mohanty et al., 2017). Despite their restriction to near-surface soil moisture measurements, several studies have demonstrated that remote sensing data can be used to successfully estimate effective SHPs at the field scale (Mohanty, 2013). For example, Santanello et al. (2007) inversely estimated soil hydraulic parameters of a semiarid watershed using the Noah land surface model by combining soil moisture evaluated using passive microwave remote sensing by NASA's push-broom microwave radiometer and active microwave RADARSAT-1 imagery with a parameter estimation algorithm and then compared the estimated and PTF-based SHPs. In another study, Steenpass et al. (2010) assimilated infrared-measured soil surface temperatures and time domain reflectometry based soil water contents to estimate SHPs for both synthetic and field-scale conditions.

Among the ground-based remote sensing techniques, cosmic-ray neutron sensing (CRNS) has shown good promise to capture soil moisture at relevant scales. Briefly, fast neutrons are produced by nuclear interactions between the incoming cosmic rays and elements of the Earth's atmosphere (Zreda et al., 2008). When they reach the soil surface, they penetrate to a certain depth and are scattered back into the atmosphere. Since fast neutrons are mainly moderated by hydrogen, the fast neutron intensity at near ground level is negatively correlated with the near-surface soil moisture. For this reason, soil moisture can be inferred from the fast neutron intensity measured by cosmic-ray neutron probes (CRNPs) (Zreda et al., 2008). The CRNP measures integral soil moisture in a circular footprint centered on a detector. This radius varies between 130 and 240 m depending on the site conditions, which is significantly larger than the typical spatial correlation length of soil moisture patterns (Western et al., 2004). The penetration depth of CRNP measurements varies between 15 cm for wet soils to 55 cm for dry soils (Schrön et al., 2017). Due to this large sample volume, the information content of CRNP data could potentially improve the estimation of effective SHPs for LSMs because the scale mismatch between sample volume and model resolution is much smaller.

The applicability of the CRNP method has been demonstrated for various land cover types, soil types, and climates, and CRNPs have been installed in several national monitoring networks (Bogena et al., 2015). The first network was established in the United States by the University of Arizona and has already deployed more than 60 CRNPs at various locations (Zreda et al., 2012). Similar networks have been established in Australia (Hawdon et al., 2014), the United Kingdom (Evans et al., 2016), and Germany (Baatz et al., 2014). To date, almost 200 stationary CRNPs have been installed worldwide (Andreasen et al., 2017). The required conversion of neutron intensity into soil moisture and the correction for important influencing factors (e.g., biomass, snow, and litter layer water content) have been described in detail in the literature (e.g., Andreasen et al., 2017; Desilets et al., 2010). Few recent studies have focused on the use of CRNP data for the estimation of SHPs with promising results. Both Finkenbiner et al. (2018) and Gibson and Franz (2018) combined CRNP data with empirical orthogonal functions to isolate spatial patterns of SHPs in selected agricultural fields. A statistical analysis confirmed that the use of CRNP data can improve the estimate of SHPs at the field scale.

Several types of neutron source models are available to study cosmic-ray neutron interactions near the soil surface. One of the most widely used models is the Monte Carlo N-Particle eXtended (MCNPX) neutron transport code (Pelowitz, 2011). Given the specified chemistry of the atmosphere and soil (e.g., soil mineralogy, soil moisture), MCNPX simulates nuclear collisions of individual, randomly generated, incoming cosmic rays and their interaction byproducts through the atmosphere and in the soil using libraries of nuclear properties. In this way, MCNPX allows accurate simulation of the number of fast neutrons that enter a defined detector volume above the ground. In an attempt to simultaneously describe the neutrons' dynamics and water flow in the unsaturated zone, Franz et al. (2012) successfully coupled MCNPX with the hydrological model HYDRUS-1D (Šimůnek et al., 2016) for calculating the effective sensor depth of a CRNP while accounting for three sources of hydrogen and their vertical variability. However, the high computational cost of this Monte Carlo based model makes it unsuited for Bayesian analysis frameworks, which require thousands of model executions. Recently, the Ultra Rapid Adaptable Neutron-Only Simulation (URANOS) model (Köhli et al., 2015) was developed to reduce the computational cost of CRNP simulations and to provide a neutron transport code tailored to environmental applications. By neglecting less relevant physical processes, URANOS is more computationally efficient than other available Monte Carlo codes while maintaining a similar accuracy in the simulation of neutron fluxes (Köhli et al., 2015). However, the computational gain is still not sufficient to justify its use in Bayesian analysis.

The forward neutron operator COSMIC has taken a major step toward the efficient integration of CRNS data in models

(Shuttleworth et al., 2013). It provides a simplified description of neutron interactions, and the use of a physically based analytical approach reduces the computational cost by four orders of magnitude compared with MCNPX. COSMIC calculates the fast neutron flux from the soil moisture profile and can be easily coupled with hydrological models. Recently, Baatz et al. (2017) were able to assimilate data from a network of CRNPs installed in the River Rur catchment into the Common Land Model (CLM4.5) to update soil moisture and SHPs of the catchment. In another study, the COSMIC and Noah models were coupled to assimilate CRNP data from the Santa Rita Range field site (Shuttleworth et al., 2013). In particular, the Noah–COSMIC model was used in conjunction with the global optimization algorithm AMALGAM (Vrugt and Robinson, 2007) to recalibrate the Noah model by minimizing the errors between simulated and observed neutron fluxes. Their results demonstrated that the assimilation of CRNP data could effectively improve the accuracy of the model predictions. To date, the only available studies on the use of CRNP data in the inverse estimation of soil hydraulic properties are those of Rivera Villarreyes et al. (2014) and Baatz et al. (2017). In the former, integral soil moisture estimates obtained for the CRNP support volume were transformed into the soil water storage for direct calibration of the effective soil hydraulic parameters using the HYDRUS-1D model. Despite the overall promising results of their study, the numerical approach based on the use of soil water storage data led to a poor approximation of the volumetric water content at different depths. In Baatz et al. (2017), soil water contents estimated from CRNS data were assimilated with the local ensemble transform Kalman filter in the CLM4.5 model to update soil texture and organic matter used in the PTFs for the estimation of the SHPs. Results of that study demonstrated the potential of CRNS networks to improve subsurface parameterization in the regional LSM. However, the use of PTFs and the indirect assimilation of CRNS data represent potential sources of additional uncertainty in the data assimilation framework.

Thus, the main aim of this study was to provide a comprehensive theoretical and experimental assessment of the information content of CRNP data for the inverse estimation of effective SHPs at the field scale. The problem was addressed in the following way. First, a combined mechanistic description of variably saturated flow and soil-neutron interactions was provided by coupling the hydrological model HYDRUS-1D and the neutron transport code COSMIC. Before proceeding with an analysis of actual CRNP data from an experimental facility in Germany, an analysis of synthetic data was performed by combining the coupled HYDRUS–COSMIC model with a Bayesian inference algorithm. The synthetic example simplified the experimental case study by describing the soil-neutrons interactions in a homogeneous soil profile and provided the first proof of concept for the estimation of SHPs from CRNP data. Finally, the actual data from a heterogeneous soil profile was used to evaluate the potential of CRNP data for the inverse estimation of SHPs under real conditions. A comparison between inverse estimation using neutron fluxes and classical point measurements of water content completes and further enriches the analysis.

Materials and Methods

Theory

Subsurface Water Flow and Root Water Uptake

The finite-element hydrological model HYDRUS-1D (Šimůnek et al., 2016) numerically solves the one-dimensional Richards equation describing variably saturated water flow in the soil profile:

$$\frac{\partial \theta}{\partial t}=\frac{\partial}{\partial z}\left[K(h)\left(\frac{\partial h}{\partial z}+1\right)\right]-S \qquad [1]$$

where θ is the volumetric water content [$L^3\ L^{-3}$], h is the soil water pressure head [L], $K(h)$ is the unsaturated hydraulic conductivity [$L\ T^{-1}$], t is time [T], z is the soil depth [L], and S is a sink term [$L^3\ L^{-3}\ T^{-1}$], defined as a volume of water removed from a unit volume of soil per unit of time due to plant water uptake. A solution of the Richards equation requires knowledge of the SHPs, which should accurately describe the hydraulic characteristics of the porous medium and its heterogeneity. It is well known that agricultural land management can significantly influence the soil structure and corresponding SHPs in the near surface. Under such circumstances, the shape of the retention curve may be constant with depth, but the soil hydraulic conductivity and porosity are expected to change significantly. Thus, in the present study, the vertical variability of the soil is described by combining the unimodal van Genuchten–Mualem (VGM) (van Genuchten, 1980) functions with the scaling factors proposed by Vogel et al. (1991). In particular, three independent dimensionless scaling factors are used: φ_θ, φ_h, and φ_K for the water content, the pressure head, and the saturated hydraulic conductivity, respectively. These three scaling parameters are used to define a linear model of the actual spatial variability in the soil hydraulic properties as follows:

$$\begin{cases}\theta(h)=\theta_r+\varphi_\theta\left[\theta^*(h^*)-\theta_r^*\right]\\ h=\varphi_h h^*\\ K(h)=\varphi_K K^*(h^*)\end{cases} \qquad [2]$$

where $\theta^*(h^*)$ and $K^*(h^*)$ are the reference soil hydraulic functions, which are ideally those unaffected by surface management activities. This theoretical approach guarantees high modeling flexibility since it can describe both homogeneous and heterogeneous soil profiles using a single set of reference soil hydraulic functions and only a few more parameters (i.e., the scaling factors). If the soil is homogeneous, the scaling factors are set to 1.

Feddes et al. (1978) defined S as

$$S(h)=a(h)S_p \qquad [3]$$

where S_p is the potential root water uptake rate and $a(h)$ is a dimensionless water stress response function that depends on the soil pressure head h and can vary between 0 and 1. Parameters of the

stress response function for a majority of agricultural crops can be found in various databases (e.g., Taylor and Ashcroft, 1972; Wesseling et al., 1991). Potential root water uptake S_p is calculated from the potential transpiration rate T_p and the root distribution function. Beer's equation is used to partition the reference evapotranspiration calculated with the Penman–Monteith equation (Allen et al., 1998) into potential transpiration and soil evaporation fluxes (e.g., Ritchie, 1972) using leaf area index information. For a detailed explanation of the partitioning of evapotranspiration, see Sutanto et al. (2012).

Cosmic-Ray Soil Moisture Interaction Code

The physically based COsmic-ray Soil Moisture Interaction Code (COSMIC) (Shuttleworth et al., 2013) is used to calculate the aboveground neutron intensity for a given soil moisture profile. COSMIC includes simple descriptions of (i) degradation of the incoming high-energy neutron flux with soil depth, (ii) creation of fast neutrons at each depth in the soil, and (iii) scattering of the resulting fast neutrons before they reach the soil surface. See Shuttleworth et al. (2013) for a detailed description of the COSMIC model.

COSMIC requires several site-independent and site-specific time-invariable parameters. In particular, the parameters L_1 = 162.0 g cm^{-2}, L_2 = 129.1 g cm^{-2}, and L_4 = 3.16 g cm^{-2} were found to be site independent (Shuttleworth et al., 2013), while the parameters L_3 (g cm^{-2}) and α (cm^3 g^{-1}) were found to be dependent on the soil bulk density ρ_b according to

$$L_3 = -31.65 + 99.29\rho_b \quad [4]$$

$$\alpha = 0.404 - 0.101\rho_b \quad [5]$$

The remaining two parameters, the lattice water content θ_l [L^3 L^{-3}] and the number of high-energy neutrons at the soil surface N_{COSMIC} (dimensionless), are also site dependent and must be measured and calibrated, respectively.

A FORTRAN version of the COSMIC code is freely available online (http://cosmos.hwr.arizona.edu). For this study, the FORTRAN code was rewritten in the Python language to enable a more efficient model coupling with HYDRUS-1D. The open-source compiler Numba (Lam et al., 2015) was used to speed up the Python code and to significantly reduce its execution time. The Python version of the COSMIC code was verified against the original FORTRAN code before further use.

Model Coupling Strategy

The COSMIC and HYDRUS models were coupled via a Python interface to dynamically calculate subsurface water flow by HYDRUS and neutron intensity by COSMIC. To this end, several user-defined Python subroutines that interact with the HYDRUS files were developed. The coupling of the two models is accomplished in the following way:

1. Model initialization: HYDRUS is initialized by setting up input data, the numerical domain, and boundary conditions. In addition, the temporal resolution of the model output for the soil moisture profile is defined, which determines the temporal resolution of the simulated neutron flux. Similarly, the COSMIC parameters are defined, and the Python code is compiled using Numba.
2. HYDRUS execution and data processing: HYDRUS-1D is externally executed directly from the Python code, and a check is performed for numerical convergence and the final mass balance error. If the simulation is successful, the calculated soil moisture profiles are read and stored in a matrix, in which rows represent the vertical discretization of the model domain and columns represent the selected time steps for soil moisture profile information.
3. COSMIC execution: The matrix of soil moisture profiles is passed to COSMIC. Two nested loops are used to iterate through depth and time and to calculate a time series of simulated aboveground neutron fluxes that can be compared with measured CRNP data.

Uncertainty Analysis

The main goal of the uncertainty analysis is to provide a statistical basis for the assessment of the information content of CRNP data for the inverse estimation of soil hydraulic parameters. This is accomplished by first using a global optimization algorithm for the identification of the global optimum, which is subsequently used as a starting point for the Bayesian uncertainty analysis based on a Markov chain Monte Carlo (MCMC) algorithm to reduce its autocorrelation time, thus improving the computational efficiency of the analysis. The global optimum is determined using the Particle Swarm Optimization algorithm (Kennedy and Eberhart, 1995).

Bayesian Inference

Global optimization algorithms are generally used to find an optimal set of parameters that maximize a likelihood function. However, different sources of uncertainty can affect hydrological data assimilation frameworks (i.e., model inadequacy, observations and measurements errors, improper boundary conditions, etc.). Therefore, there is no reason to assume that a single optimized parameter set represents the only realistic model realization. It is more reasonable to consider it as one of many acceptable solutions of the problem. This idea underpins the *equifinality* concept first introduced by Beven and Binley (1992) in the early 90s, which emphasizes the fact that there are many acceptable (i.e., *behavioral*) representations that cannot be excluded from the analysis and that should be considered when quantifying the uncertainty associated with model predictions.

Several methods have been proposed in the literature to assess the model predictive uncertainty (e.g., Beven and Binley, 1992; Kavetski et al., 2006; Vrugt et al., 2008a). However, during the last decade, the scientific community has focused on the application of statistically rigorous Bayesian methods for the calibration of hydrological models. To explain the Bayesian approach, let us consider a HYDRUS–COSMIC model realization with a symbol $\mathbf{Y}$, which is a function of q model parameters, $\mathbf{u} = \{u_1, u_2, ..., u_q\}$:

$$\mathbf{Y} = f(\mathbf{u}) \quad [6]$$

Bayes' theorem combines the prior knowledge about the investigated process with the observed data to obtain the posterior distribution of the parameters. In a probabilistic context, this can be written as

$$\begin{aligned} &\Pr(\tilde{\mathbf{Y}}|\mathbf{u}) \times \Pr(\mathbf{u}) = \Pr(\tilde{\mathbf{Y}}) \times \Pr(\mathbf{u}|\tilde{\mathbf{Y}}) \\ &\text{Likelihood} \times \text{Prior} = \text{Evidence} \times \text{Posterior} \\ &L(\mathbf{u}) \times \pi(\mathbf{u}) d\mathbf{u} = Z \times p(\mathbf{u}) d\mathbf{u} \end{aligned} \quad [7]$$

where $\tilde{\mathbf{Y}}$ are the observed data, which modulate our prior belief $\pi(\mathbf{u})d\mathbf{u}$ into the posterior $p(\mathbf{u})d\mathbf{u}$. One of the main goals of Bayesian analysis in hydrological model calibration is the estimation of the parameters' posterior distribution. This is usually accomplished by applying MCMC algorithms. One of the main problems faced in the Bayesian analysis of hydrological models is their strong nonlinearity and their discontinuous nature, which makes it very difficult to apply efficient MCMC algorithms such as Hamiltonian Monte Carlo sampling (Betancourt, 2017). Although the classic Metropolis–Hastings algorithm (Metropolis et al., 1953) is easy to implement, it is unable to deal with highly correlated and multimodal posteriors often encountered in the calibration of hydrological models. Thus, a variety of MCMC algorithms have been developed and successfully applied in water-related problems in recent years.

In this study, we use the Affine Invariant Ensemble Sampler (AIES), which was first proposed by Goodman and Weare (2010). The AIES algorithm is an ensemble MCMC algorithm that has proven to be extremely effective when the dimensionality of the problem is not very high (Huijser et al., 2015), as is the case in this study. Each ensemble, Ω, consists of D walkers, which can be considered as a vector in the q-dimensional parameter space. The core of AIES is its affine invariance property, which implies that the performance of the method is independent of the aspect ratio in highly skewed distributions. This is a highly desirable property when calibrating hydrological models because of the prevalence of highly correlated posterior distributions. In AIES, the ensemble Markov chain is evolved using a *stretch move* step (Goodman and Weare, 2010), which significantly reduces the chain's autocorrelation time. Briefly, the main idea is that the ensemble carries useful information about the approximated distribution, and thus each walker is updated using a complementary ensemble. A parameter a, which is usually set to 2.0 (Foreman-Mackey et al., 2012), is used to "stretch" the proposal. For a thorough description of the AIES, see Goodman and Weare (2010), Foreman-Mackey et al. (2012), and Huijser et al. (2015). It is worth noting that this study is the first one that uses the AIES algorithm in a hydrological context.

One of the main advantages of AIES is that it requires the specification of only two parameters, i.e., the stretch factor, a, and the number of walkers, D. There are no clear indications in the literature about the best values of D and a, and they typically depend on the investigated problem. Based on some preliminary tests, D and a were set to $10q$ (q is the number of model parameters) and 2.0, respectively. In this study, the Python package *emcee* (Foreman-Mackey et al., 2012) is coupled with the HYDRUS–COSMIC model to carry out the Bayesian analysis. *Emcee* is a stable and well-tested Python implementation of the AIES method that includes several MCMC convergence diagnostic tools. The walkers are initialized by random sampling from a multivariate normal distribution centered on the global optimum with a diagonal covariance matrix characterized by a small standard deviation of 0.01. Such an initialization around the global optimum is expected to reduce the autocorrelation time, thus increasing the overall computational efficiency of the analysis.

The AIES algorithm calls the coupled HYDRUS–COSMIC model at each iteration. However, the stochastic combination of various SHPs can lead to non-convergent model runs for HYDRUS-1D, mainly due to the inability to appropriately adjust the HYDRUS-1D settings (e.g., mesh size) during the Monte Carlo analysis. In this study, non-convergent runs are identified and an unrealistically large value is attributed to the sum of squared residuals. This procedure, which is similar to what was reported by Brunetti et al. (2016) and Wöhling and Vrugt (2011), can significantly slow down the convergence of the AIES because it introduces sudden and unrealistic jumps in the response surface due to the artificially low value of the likelihood. In future work, regularization of the response surface could be considered through a local interpolation or a surrogate model (e.g., Brunetti et al., 2017).

A non-informative uniform prior is used for all parameters in the uncertainty analysis. The only information provided by this prior are the bounds of the feasible parameter space. Within these bounds, all parameter values have the same probability. The bounds were set based on field measurements (e.g., particle size distribution) and literature values.

Markov Chain Monte Carlo Diagnostic

Goodman and Weare (2010) suggested using the integrated autocorrelation time (IAT), τ_{int}, to assess the accuracy of the AIES. The IAT is the number of steps (i.e., ensemble moves) required for the walker to produce an independent sample. This number is expected to be relatively large if the walkers are initialized in a distribution that is not equal to the stationary distribution. Such a transient period is usually defined as *burn-in* and should be discarded from the analysis. In the present study, the burn-in period is assumed to be $2\tau_{int}$. It is worth noting that we avoid the use of the widely applied Gelman–Rubin test because walkers in the AIES are not formally independent.

The IAT determines statistical errors in the Monte Carlo analysis once a stationary distribution has been attained (Sokal, 1996). In particular, the statistical error ε of the mean of the posterior depends on τ_{int} and is calculated as

$$\varepsilon = \sqrt{\frac{2\tau_{int}}{Dm}} \quad [8]$$

where m is the number of steps. Obviously, a larger sample reduces the errors but significantly increases the computational time. Thus,

in this study, the admissible maximum statistical error was set to 5%, which should guarantee a good trade-off between numerical accuracy and computational effort.

The estimation of the IAT is notoriously difficult because it is a two-point statistic. More specifically, the IAT should asymptotically reach its true value for a large number of samples. Thus, a preliminary IAT convergence analysis is performed to assess its calculated value. This is accomplished in the following way:

- The AIES algorithm is preliminary run for 3000 steps to obtain a significant statistical sample. This requires a few days of computation time considering that the execution time of the HYDRUS–COSMIC model is <1 s.
- Each walker is divided into 20 parts, and the IATs are calculated for increasing chain lengths. We adopt the numerical procedure described by Sokal (1996). In particular, a mean normalized autocorrelation function is computed by averaging the normalized autocorrelation functions calculated for each walker in the ensemble. Then, the procedure described by Sokal (1996) is used to estimate the IAT for each soil hydraulic parameter. The IAT is expected to exhibit a logarithmic growth.
- The analysis is assumed to converge if

$$\begin{cases} \varepsilon_{\max} < 5\% \\ m > 10\tau_{\text{int}}^{\max} \end{cases} \quad [9]$$

  Otherwise more samples are generated by evolving the AIES. The second condition in Eq. [9] is meant to reduce the MCMC error and mitigate the effect of an imperfect estimation of the IAT.

Likelihood Function

If we assume that the error residuals are uncorrelated and normally distributed with constant variance, σ^2, the likelihood function $L(\mathbf{u})$ can be written as

$$L(\mathbf{u}) = \prod_{i=1}^{k} \frac{1}{\sqrt{2\pi\sigma^2}} \exp\left\{ -\frac{1}{2}\sigma^2 \left[y_i(\mathbf{u}) - \tilde{y}_i \right]^2 \right\} \quad [10]$$

where $y_i(\mathbf{u})$ and $\tilde{y}_i(\mathbf{u})$ are the ith model realization and its corresponding measured value, respectively. For algebraic simplicity, the log-likelihood $\ell(\mathbf{u})$ is used:

$$\ell(\mathbf{u}) = -\frac{k}{2}\ln(2\pi) - \frac{k}{2}\ln\left(\sigma^2\right) - \frac{1}{2\sigma^2}\sum_{i=1}^{k}\left[y_i(\mathbf{u}) - \tilde{y}_i \right]^2 \quad [11]$$

Equation [11] is used in the inverse modeling with synthetic data because the error variance is known. In the inverse modeling with measured data, σ^2 is treated as a nuisance parameter and integrated out from the inference equation (e.g., Kavetski et al., 2006). The new likelihood is then written as

$$\ell(\mathbf{u}) = -\frac{k}{2}\ln\left\{ \sum_{i=1}^{k}\left[y_i(\mathbf{u}) - \tilde{y}_i \right]^2 \right\} \quad [12]$$

Rollesbroich Grassland Experimental Catchment

The Rollesbroich grassland experimental catchment is located in western Germany in the Eifel mountain range and is part of the TERENO observatory Eifel/Lower Rhine Valley (Bogena et al., 2012, 2018). It covers an area of about 40 ha with altitudes ranging from 474 to 518 m asl (the average slope is 1.63°). The mean annual air temperature and precipitation are 7.7°C and 1033 mm, respectively. The vegetation is dominated by perennial ryegrass (*Lolium perenne* L.) and smooth meadow grass (*Poa pratensis* L.), and the predominant soils are Cambisols in the southern part and Stagnosols in the northern part of the catchment. All components of the water balance (e.g., precipitation, evapotranspiration, runoff) are continuously monitored using state-of-the-art instrumentation. A detailed description of the instrumentation at the Rollesbroich experimental catchment and available hydrological datasets was given by Qu et al. (2016). A SoilNet wireless network (Bogena et al., 2010) with more than 500 soil moisture sensors (ring oscillator probes, Bogena et al., 2017) was installed in May 2011 to measure the soil water content at depths of 5, 20, and 50 cm (Qu et al., 2014) at 87 locations. In particular, two sensors were installed in parallel at each depth with a distance of ~10 cm to increase the sensing volume and to allow examination of inconsistencies in sensor reading. In May 2011 and May 2012, two CRNPs (Type CRS1000, HydroInnova LLC) were installed in the southern and northern parts of the catchment. The CRNP calibration and a comparison with in situ soil water content data obtained with SoilNet were presented in Baatz et al. (2014). This study uses data only from the CRNP located in the southern part of the catchment.

A 6-mo-long dataset (1 Apr. 2012–30 Sept. 2012) was selected for further analysis (Fig. 1). In particular, daily precipitation and reference evapotranspiration were used as input data in HYDRUS for both synthetic and experimental scenarios, while daily measured water contents at three depths (i.e., z = −5, −20, and −50 cm) and the aboveground neutron fluxes were used in the inverse estimation of the soil hydraulic parameters in the experimental scenarios.

Numerical Domain and Boundary Conditions

The 200-cm-deep soil profile was discretized in HYDRUS-1D into 100 finite elements, refined at the top to accommodate pressure head gradients induced by the atmospheric conditions. An atmospheric boundary condition is applied at the soil surface using (i) precipitation and potential evaporation fluxes, (ii) a prescribed zero pressure head (i.e., full saturation) during ponding, and (iii) equilibrium between the soil surface pressure head and the atmospheric water vapor pressure when the atmospheric evaporative demand cannot be met. The effect of groundwater was not simulated in this study and thus a free-drainage boundary condition was used at the bottom of the model domain (z = −200 cm).

The initial pressure head was assumed to be constant and equal to −100 cm in the entire model domain. A 3-mo-long spin-up period was used to limit the influence of the initial condition on the simulation results. Three observation points were set at depths of −5, −20, and −50 cm to retrieve simulated volumetric water contents.

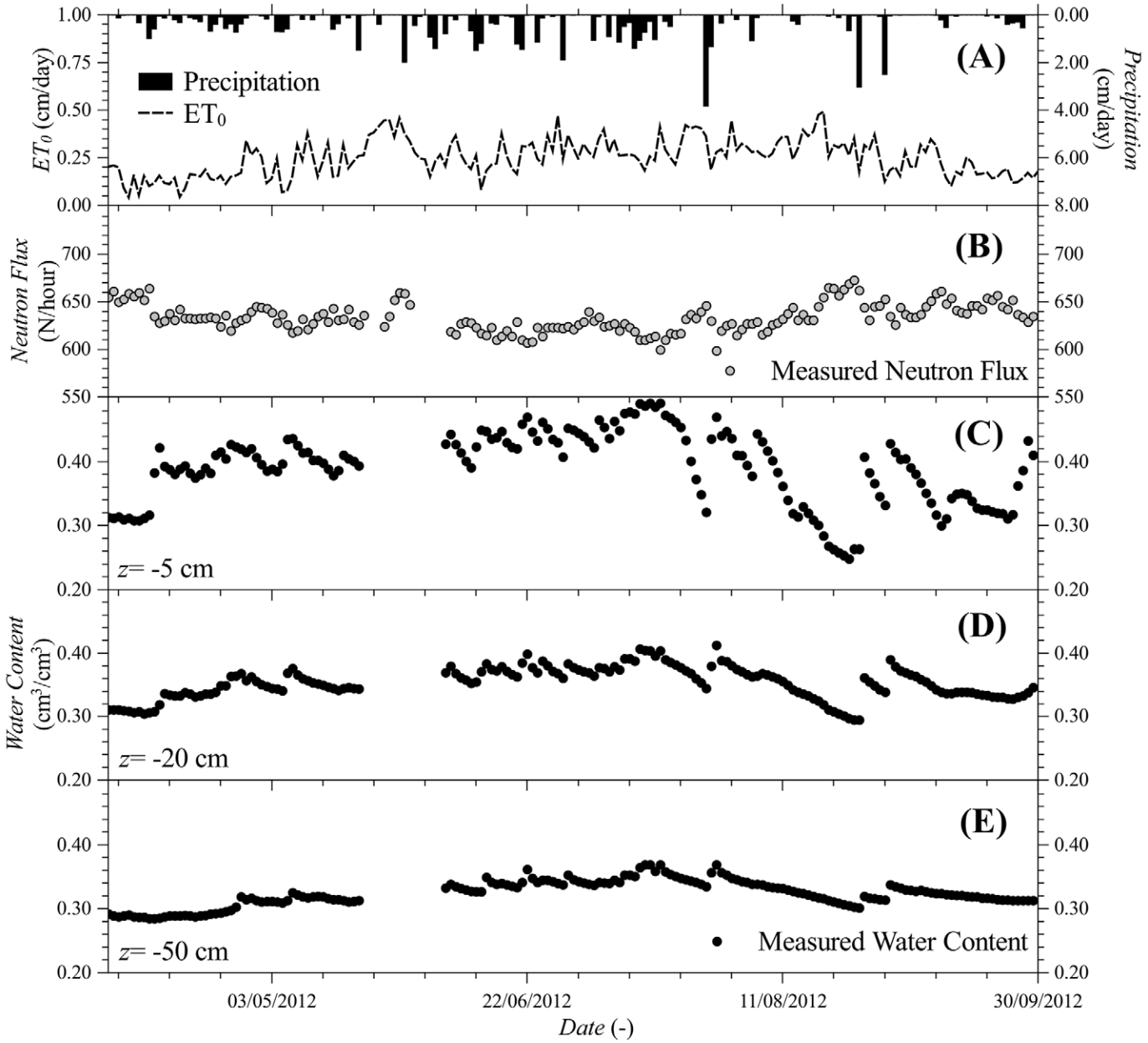

Fig. 1. (A) Precipitation (bars) and reference evapotranspiration ET_0 (dashed line) used as input data in HYDRUS, and (B) measured neutron fluxes and (C,D,E) water contents at three depths in the Rollesbroich catchment between April and September 2012.

Inverse Estimation with Synthetic Data

Several studies have demonstrated how data assimilation frameworks can be significantly affected by various sources of uncertainty at the field scale that can lead to biased conclusions if not properly accounted for in the analysis (Mantovan and Todini, 2006; Mockler et al., 2016; Montanari, 2007). Because the main aim of this study was to provide an objective evaluation of the information content of the CNRP data for the inverse estimation of SHPs at the field scale, it was important to first analyze synthetic modeling scenarios that are not affected by uncertainty in the model structure and measurement errors before analyzing actual experimental data. Here, the synthetic modeling scenario is a simplification of the experimental case study and is focused on soil-neutron interactions in a homogeneous sandy soil. The strongly unsaturated conditions induced by the use of a sandy soil will increase the aboveground neutron intensity and thus provide different information than the experimental case study characterized by a silty soil.

Model Setup

Variably saturated water flow is simulated in a 200-cm-deep homogeneous loamy sand soil profile covered by grass. The VGM parameters reported by Carsel and Parrish (1988) for loamy sand were used to generate the synthetic dataset. The scaling factors were fixed to 1.0 to obtain a homogeneous soil profile. The rooting depth and density were assumed to be 15 cm and 1.0, respectively,

while a constant leaf area index of 2.0 (Qu et al., 2016) was used to partition reference evapotranspiration. The Feddes parameters for grass were chosen according to Taylor and Ashcroft (1972) and Wesseling et al. (1991). The COSMIC parameters were set according to Baatz et al. (2014) (Table 1).

The synthetic dataset was generated in the following way. First, a forward numerical simulation by the HYDRUS-1D model was used to generate a time series of the volumetric water content at $z = -5$ cm and daily soil moisture profiles. The latter were passed to the COSMIC model for the simulation of the aboveground neutron fluxes. Next, synthetic noise was added to the original time series. The selection of σ values has a significant influence on parameter uncertainty and thus they should be properly set to reflect the accuracy of real measured data. Indeed, an unbalanced choice of such values can lead to biased conclusions on the information content of the investigated data. These values were thus set in this study based on a preliminary analysis of the noise in selected measured datasets. Briefly, a spectral analysis based on the Fast Fourier Transform was used to separate the deterministic (signal) and stochastic (noise) components of the measured neutron fluxes and volumetric water contents. The Shapiro–Wilk test was then used to assess the normality of the noise, and the standard deviations were calculated. Based on this analysis, random noise with zero mean and standard deviations equal to 30.0 N h^{-1} and 0.01 cm^3 cm^{-3} for the neutron flux and water content time series, respectively, was used. The input, original, and synthetic data for the selected time period are shown in Fig. 2.

Table 1. The COSMIC parameters used in the synthetic and experimental scenarios (Baatz et al., 2014).

Scenario	ρ_{bd}†	θ_l	N_{COSMIC}	L_1	L_2	L_4
	g cm^{-3}					
Synthetic	1.42	0.037	189	161.98	129.14	3.16
Experimental	1.09	0.068	213	161.98	129.14	3.16

† ρ_{bd}, soil bulk density; θ_l, lattice water content; N_{COSMIC}, number of high-energy neutrons at the soil surface; L_1, L_2, and L_3, empirical parameters.

Synthetic Modeling Scenarios

Three synthetic modeling scenarios are considered for the inverse estimation of soil hydraulic parameters (Table 2). Scenarios S1 and S2 examine the information content of the temporal evolution of aboveground neutron flux and water content, respectively, at one observation point. The comparison of the parameter uncertainty obtained by these two scenarios will clarify the potential of CRNP data to estimate SHPs compared with traditional point measurements. Scenario S3, which combines the two synthetic datasets, is used to investigate the effect of the joint inversion of water content and neutron flux data. The parameter bounds used in this analysis are reported in Table 3.

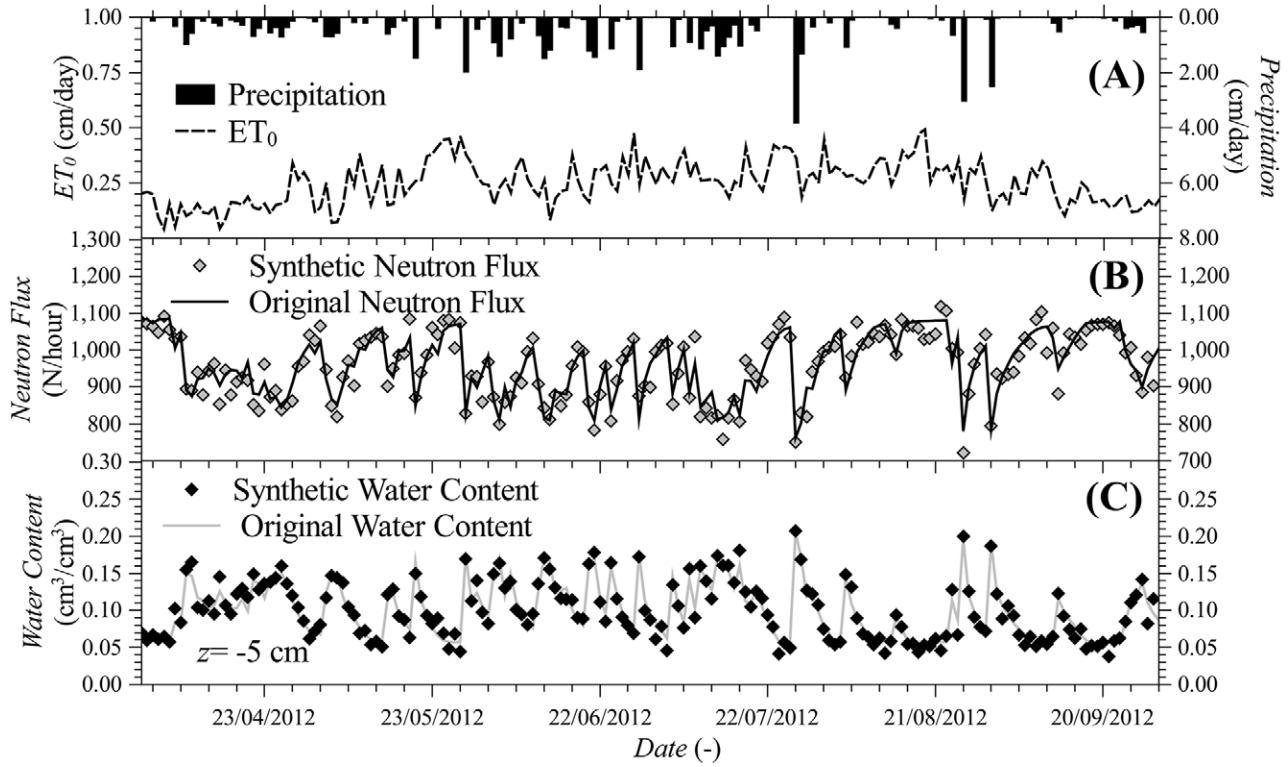

Fig. 2. (A) Precipitation (bars) and reference evapotranspiration ET_0 (dashed line) from the Rollesbroich catchment used as input data in HYDRUS, and simulated (solid lines) and synthetic (with added noise, diamonds) (B) neutron fluxes and (C) water contents at depth $z = -5$ cm between April and September 2012.

Inverse Estimation with Actual Data

Model Setup

Measured particle size distributions reported by Qu et al. (2016) for the Rollesbroich catchment revealed negligible differences in the textural composition of the soil at different depths. On the other hand, bulk densities increased with depth from 0.94 to 1.52 g cm^{-3}, and porosities decreased with depth from 0.65 and 0.43 cm^3 cm^{-3}. This vertical soil variability can be attributed to prior agricultural land management (i.e., the plow layer is 20–30 cm thick), which reduced the compaction of the surface layer. The measured soil properties highlight the existence of two different soil horizons in the top layer (i.e., $z > -30$ cm). Indeed, the porosity and the bulk density for $z > -10$ cm are 20% higher and 25% lower, respectively, than for the underlying topsoil. Thus, three soil materials are assumed in the model: Soil Material 1 extends to $z = -10$ cm; Soil Material 2 ranges from −10 to −30 cm; and Soil Material 3 extends below −30 cm. Since Soil Material 3 is not affected by agricultural land management, the scaling factors were set to 1.0 for this material.

The pedotransfer model ROSETTA (Schaap et al., 2001) was used to identify the plausible ranges of the soil hydraulic parameters and the scaling factors. On the basis of this analysis, the water content scaling factors φ_θ were fixed to 1.4 and 1.1 for Soil Materials 1 and 2, respectively, thus reducing the dimensionality of the inverse problem. Because the residual water content exhibited low variability, it was fixed to 0.07, which is a common value for silty soils. The tortuosity and pore-connectivity parameter L (dimensionless) in the VGM equation was set to 0.5 in all numerical simulations. The aforementioned model simplifications reduced the number of unknown parameters to eight. The parameter bounds used in the analysis are reported in Table 3.

Experimental Modeling Scenarios

Three experimental data analysis scenarios are considered (Table 2). Scenarios E1 and E2, in analogy to Scenarios S1 and S2, consider only measured neutron flux and near-surface water content (i.e., $z = -5$ cm), respectively. The comparison of these two scenarios will clarify the information content of the CRNP data to estimate SHPs in layered soils relative to near-surface point measurements. In addition, Scenario E3 uses measured water contents at three different depths (i.e., $z = -5$, −20, and −50 cm). This scenario should provide more accurate estimates of SHPs because of the higher amount of measurements in multiple soil layers and thus serves as a benchmark for the other two scenarios.

Table 2. Synthetic modeling and experimental data analysis scenarios.

Data	Scenario	
	Synthetic (homogeneous soil)	Experimental (heterogeneous soil)
Aboveground neutron flux time series	S1	E1
Near-surface water content time series ($z = -5$ cm)	S2	E2
Three water content time series ($z = -5$, −20, and −50 cm)	–	E3
Near-surface water content and neutron flux time series	S3	–

Results and Discussion

Inverse Estimation with Synthetic Data

Markov Chain Monte Carlo Diagnostic

The development of the IAT in the MCMC analyses for the three synthetic scenarios is reported in Fig. 3. The asymptotic behavior of the IAT with increasing algorithmic steps suggests that a reliable estimation has been obtained for all three scenarios. It can be seen that all three scenarios exhibit similar autocorrelation times. In particular, the dynamics of the IAT indicate that approximately 100 ensemble moves (i.e., steps) are sufficient for the AIES to forget about its initial position and to start sampling from a stable posterior distribution. The saturated water content exhibits the largest IAT in Scenarios S1 and S2 (Fig. 3A and 3B), while in Scenario S3 (Fig. 3C) it is slightly larger for the shape parameter n. The short autocorrelation times lead to a maximum statistical error of the Monte Carlo analyses (Eq. [8]) of approximately 3.5% after 3000 steps. This is well below the prescribed tolerance of 5%, thus indicating a good accuracy in the estimation of the posterior distributions.

Uncertainty Analysis

The joint and marginal posterior distributions for each soil hydraulic parameter for Scenario S1 (aboveground neutron fluxes) are shown in Fig. 4. The inverse problem is markedly unimodal, with strong parameter interactions. More specifically, the joint

Table 3. The bounds of the van Genuchten–Mualem parameters and their true values used in the synthetic and experimental scenarios.

Parameter†	Synthetic			Experimental	
	Lower bound	Upper bound	True value (Carsel and Parrish, 1988)	Lower bound	Upper bound
θ_r, cm^3 cm^{-3}	0.03	0.08	0.06	0.07	0.07
θ_s, cm^3 cm^{-3}	0.35	0.45	0.41	0.30	0.45
$\log_{10}\alpha$, cm^{-1}	−1.50	−0.50	−0.91	−2.50	−0.85
n	1.50	3.00	2.28	1.10	2.00
$\log_{10}K_s$, cm d^{-1}	1.00	3.00	2.54	0.50	3.00
φ_{h1}	1.00	1.00	1.00	1.00	5.00
φ_{h2}	1.00	1.00	1.00	1.00	5.00
φ_{K1}	1.00	1.00	1.00	1.00	20.00
φ_{K2}	1.00	1.00	1.00	1.00	5.00

† θ_r, residual water content; θ_s, saturated water content; α and n, shape parameters; K_s, saturated hydraulic conductivity, φ_{h1} and φ_{K1}, and φ_{h2} and φ_{K2}, pressure head and saturated hydraulic conductivity scaling factors for Soil Materials 1 and 2, respectively.

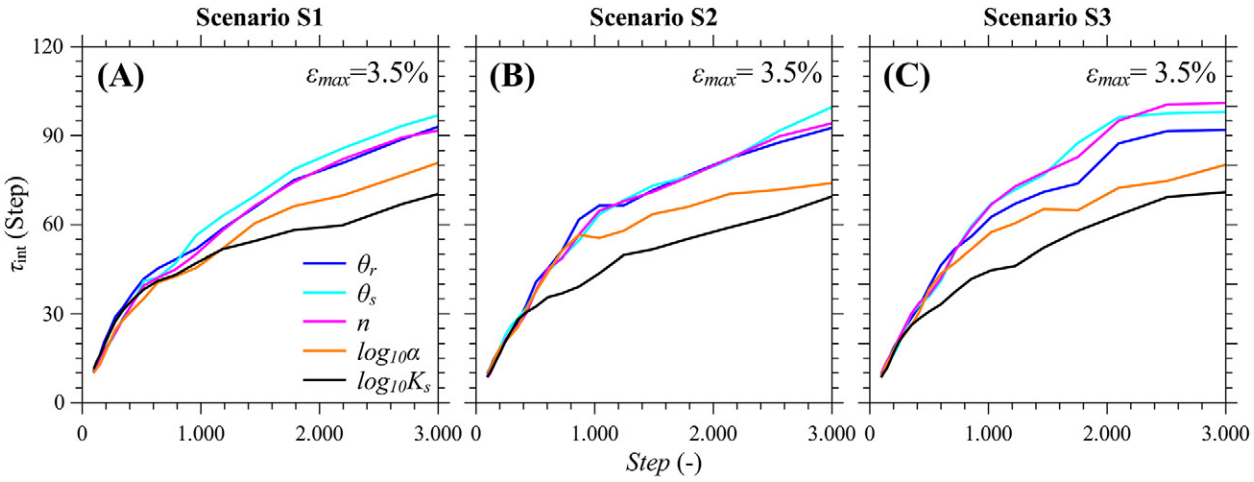

Fig. 3. The diagnostic plot of the Affine Invariant Ensemble Sampler (AIES) algorithm for synthetic modeling scenarios showing the integrated autocorrelation time τ_{int} against the algorithm step for the soil hydraulic parameters of residual soil water content (θ_r), saturated soil water content (θ_s), the van Genuchten–Mualem parameters n and α, and saturated hydraulic conductivity (K_s), along with the maximum statistical error (ε_{max}) for Scenarios (A) S1, (B), S2, and (C) S3.

posterior distribution of θ_s and K_s reveals an expected positive correlation, while the VGM shape parameters are negatively correlated. The interdependence of α and n is exacerbated, as indicated by their slight banana-shaped joint posterior distribution. Interestingly, the posterior for K_s is unimodal, even though it spans a relatively broad range of values from 83 and 602 cm d^{-1}. On the other hand, the marginal posterior distribution for θ_s is flat, indicating that the neutron data do not contain enough information content to update the uniform prior distribution. This is caused mainly by the fact that the soil water content is relatively low (0.05–0.20 m^3 m^{-3}) in these synthetic data due to the use of a highly permeable loamy sand. Therefore, water content never approaches the saturated water content of 0.41 and little information is available to constrain θ_s. Different results would probably have been obtained for other (finer) soil textures. In this case, independent measurements of soil porosity would be needed to better constrain θ_s. The strong interaction effect shown in the joint posterior θ_s–K_s suggests the impossibility of fixing the saturated water content independently from the saturated hydraulic conductivity. As expected in strongly unsaturated conditions, θ_r is precisely estimated. Similarly to θ_s, different types of K_s measurements are needed to reduce the uncertainty. Similar findings were reported by Gibson and Franz (2018), who used a mobile CRNP to quantify spatial patterns of SHPs across a range of spatial scales. In that study, the researchers underscored how an inability to map near-saturated soil water contents increased the uncertainty in the estimation of K_s.

Overall, the marginal posterior distributions indicate a well-posed inverse problem characterized by acceptable parameter identifiability and moderate uncertainty. This is confirmed by the Bayesian credible intervals reported in Table 4. In particular, the shape parameters α and n are generally well predicted, with the latter exhibiting a slightly narrower posterior distribution.

As shown in Fig. 5, the use of near-surface water content instead of neutron flux (Scenario S2) leads to similar posterior distributions. Again, the inverse problem is mostly unimodal and affected by significant parameter correlations that are similar to those in S1 (i.e., a positive correlation between θ_s and K_s, and a negative correlation between α and n). The residual water content θ_r is generally uncorrelated, except for a slight interdependence with n. As in Scenario S1, the near-surface water content measurements do not provide enough information to estimate θ_s. The marginal posterior distribution for K_s again is unimodal and spans values between 100 and 1000 cm d^{-1}, thus indicating a somewhat higher uncertainty than in Scenario S1. This effect could be related to the increased information content of the neutron flux, which is representative of the soil moisture dynamics in the entire topsoil and not just for a specific depth (i.e., 5 cm in this study).

Overall, a comparison of Fig. 4 and 5 suggests a minor decrease in parameter uncertainty for Scenario S2 compared with Scenario S1 (Table 4). This is particularly evident for the VGM shape parameters,

Table 4. Original values and 95% Bayesian credible intervals of the soil hydraulic parameters for the three synthetic scenarios. The 2.5 and 97.5% quantiles are the bounds of the credible intervals.

	Scenario						
	S1		S2		S3		True value (Carsel and Parrish, 1988)
Parameter†	2.5%	97.5%	2.5%	97.5%	2.5%	97.5%	
θ_r, cm^3 cm^{-3}	0.05	0.06	0.05	0.06	0.05	0.06	0.057
θ_s, cm^3 cm^{-3}	0.35	0.44	0.35	0.44	0.35	0.44	0.41
$\log_{10}\alpha$, cm^{-1}	−1.36	−0.66	−1.19	−0.7	−1.19	−0.76	−0.91
n	2.08	2.88	1.97	2.63	2.06	2.66	2.28
$\log_{10}K_s$, cm d^{-1}	1.92	2.78	2.06	2.93	2.00	2.86	2.54

† θ_r, residual water content; θ_s, saturated water content; α and n, shape parameters; K_s, saturated hydraulic conductivity.

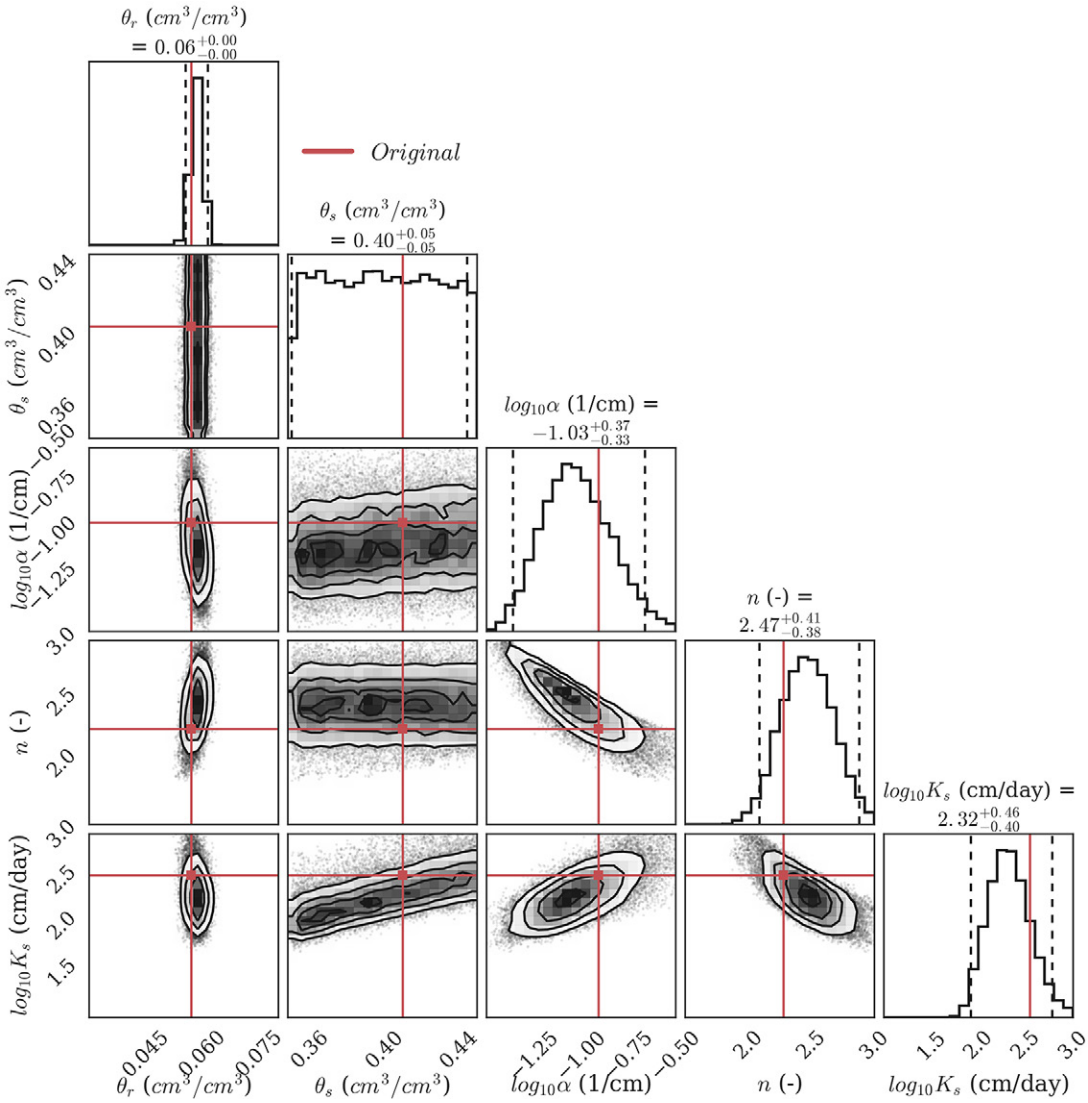

Fig. 4. Joint (below diagonal) and marginal (diagonal) posterior distributions of the soil hydraulic parameters of residual soil water content (θ_r), saturated soil water content (θ_s), the van Genuchten–Mualem parameters n and α, and saturated hydraulic conductivity (K_s) for Scenario S1. The red lines indicate the original values of the parameters for the loamy sand, while the isolines indicate 12, 39, 68, and 84% probability levels. The dashed lines indicate the Bayesian credible intervals. The axis ranges correspond to the parameter bounds reported in Table 3.

which have narrower Bayesian credible intervals and a good agreement between the most probable and true values. However, it must be noted that these differences depend on the selected level of synthetic noise used to generate the synthetic datasets. In this view, the sensor accuracy, as well as different sources of noise, plays a fundamental role in the analysis of experimental data. Similar to Scenario S1, the results suggest the need to use more informative prior distributions and to combine different data types to reduce the overall parameter uncertainty. This is investigated in Scenario S3, where both aboveground neutron fluxes and water contents are used.

The MCMC analysis for Scenario S3 (with both near-surface water contents and aboveground neutron fluxes) resulted in strongly unimodal and narrow posterior distributions (Fig. 6). The correlations between parameters are similar to those for Scenarios S1 and S2, and the relatively high uncertainty in the estimation of θ_s remains. The θ_r is precisely estimated, while the uncertainty for K_s persists. The overall reduction in the parameter uncertainty for Scenario S3 is visually evident by comparing the joint posterior distributions shown in Fig. 4, 5, and 6, and is further confirmed by the comparison of the Bayesian credible intervals (Table 4). Indeed, the VGM shape parameters have narrower credible intervals, suggesting that the simultaneous use of more and different data types reduces the uncertainty in the estimated parameters. The results of Scenario S3 further confirm that the saturated water content and hydraulic conductivity cannot be precisely inferred from data representative of strongly unsaturated conditions and that independent measurements of soil porosity and hydraulic conductivity may be needed in such a case.

As a result of this analysis, a number of conclusions can be drawn:

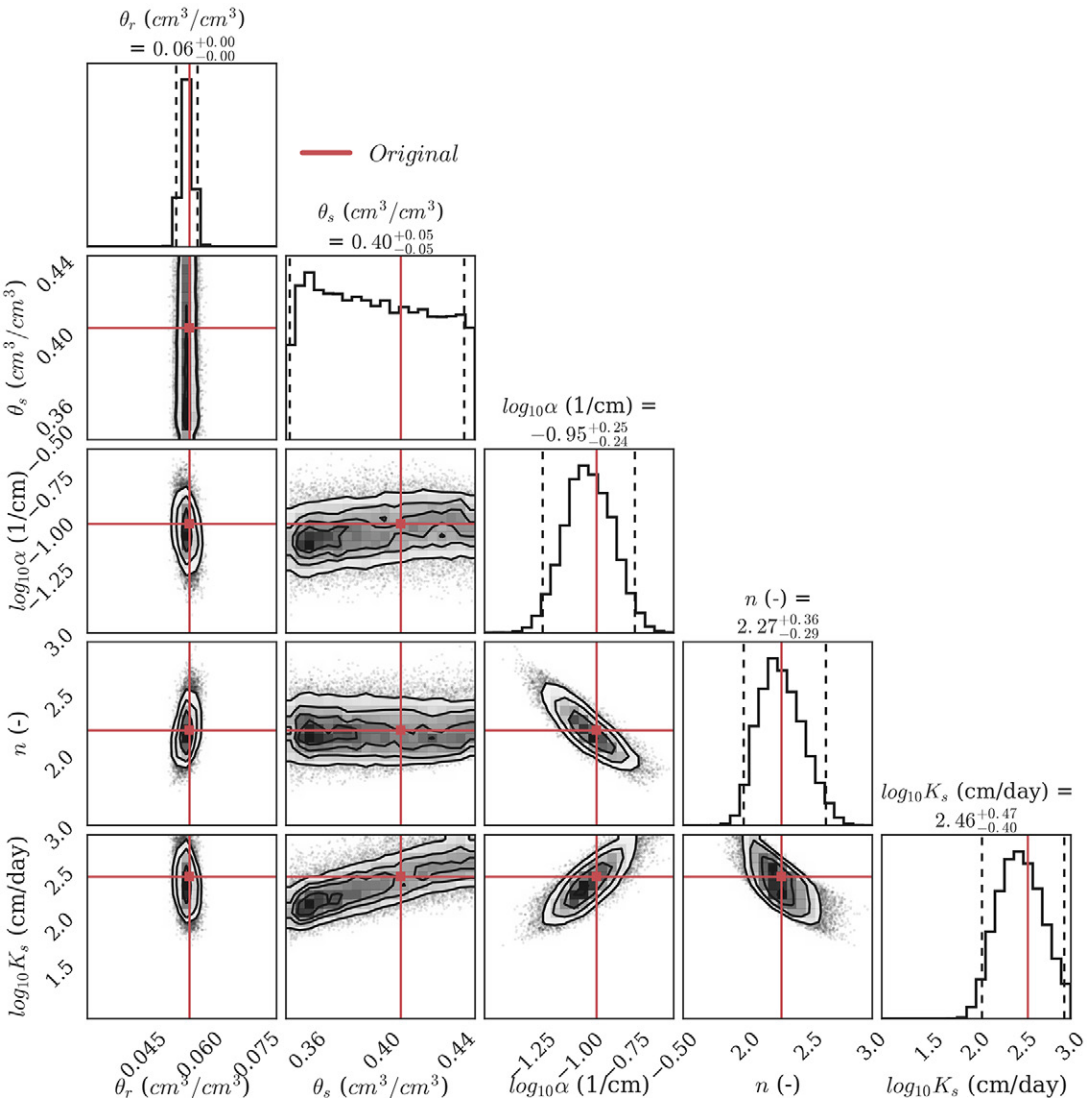

Fig. 5. Joint (below diagonal) and marginal (diagonal) posterior distributions of the soil hydraulic parameters of residual soil water content (θ_r), saturated soil water content (θ_s), the van Genuchten–Mualem parameters n and α, and saturated hydraulic conductivity (K_s) for Scenario S2. The red lines indicate the original values of the parameters for the loamy sand, while the isolines indicate 12, 39, 68, and 84% probability levels. The dashed lines indicate the Bayesian credible intervals. The axis ranges correspond to the parameter bounds reported in Table 3.

- The three synthetic datasets provided sufficient information content to obtain a satisfactory estimate of the SHPs. More specifically, the residual water content, the VGM shape parameters, and the saturated hydraulic conductivity exhibited unimodal posterior distributions, with the latter characterized by a higher uncertainty. The saturated water content could not be inferred from the dataset (for loamy sand), suggesting that independent measurements of the soil porosity are needed to better constrain the inverse problem for this soil texture.
- The use of the aboveground neutron flux data led to a satisfactory estimate of SHPs. In particular, the use of neutron flux data slightly reduced the uncertainty in the estimation of K_s. This provides the first proof of concept for the use of CRNP data for the inverse estimation of effective SHPs at the field scale.
- The simultaneous use of water content and neutron flux data reduced the parameter uncertainty. This suggests that the combination of CRNP data with sparse point measurements in the near-surface environment could reduce parameter uncertainty, in particular for the VGM shape parameters. However, the number of point measurements should be sufficient to characterize the soil heterogeneity within the CRNP footprint.

Inverse Estimation with Actual Data

Markov Chain Monte Carlo Diagnostic

The IAT values for the MCMC analyses for the three experimental scenarios are shown in Fig. 7. The maximum statistical error ranges between 3 and 5%, which is under the prescribed tolerance and indicates a reliable estimation of the posterior distributions. As expected, the increased dimensionality of the inverse problem resulted in longer autocorrelation times and more steps before convergence to the true posterior distribution. This behavior agrees

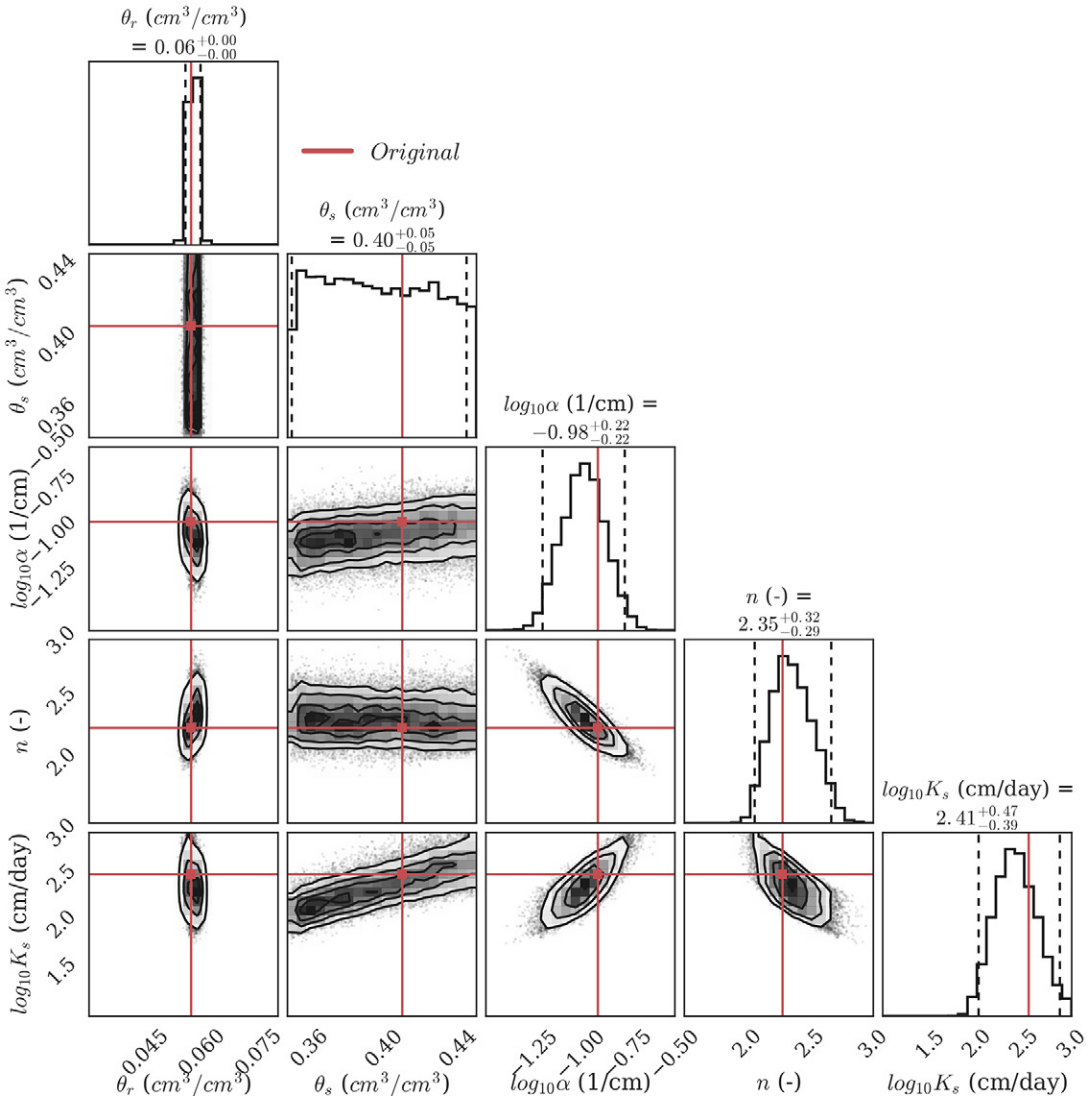

Fig. 6. Joint (below diagonal) and marginal (diagonal) posterior distributions of the soil hydraulic parameters of saturated soil water content (θ_s), the van Genuchten–Mualem parameters n and α, saturated hydraulic conductivity (K_s) for Scenario S3. The red lines indicate the original values of the parameters for the loamy sand, while the isolines indicate 12, 39, 68, and 84% probability levels. The dashed lines indicate the Bayesian credible intervals. The axis ranges correspond to the parameter bounds reported in Table 3.

with the properties of the AIES algorithm in high dimensions reported by Huijser et al. (2015).

The maximum IAT for Scenario E2 (Fig. 7B) is approximately three times larger than the IAT obtained for Scenarios E1 and E3, thus indicating convergence issues. This is related to multimodal posterior distributions, discussed below. Poor convergence is particularly evident for the scaling factor φ_{K1}, which is characterized by an IAT of 1600 steps. Under such circumstances, the ensemble samplers are known to perform poorly, mainly due to their inability to traverse low-probability valleys between peaks (Matthews et al., 2017). It is worth noting that the performance of the AIES for Scenario E2 was insensitive to the value of the stretch factor a, which was then set to the suggested value of 2.0. Future work should consider using multimodal nested sampling techniques (Feroz et al., 2009), which were found to be effective for such types of inverse problems. On the other hand, the relatively large autocorrelation time for the shape parameter n in Scenario E1 (Fig. 7A) is partially related to the position of the high-likelihood region, which is close to the boundary of the numerical domain. Indeed, bounded prior distributions can lead to convergence issues when the posterior develops near the boundary.

Uncertainty Analysis

Because Scenario E3 serves as a benchmark for the other two scenarios, this will be discussed first. The joint and marginal posterior distributions of the SHPs for this scenario are shown in Fig. 8 and have a markedly unimodal pattern characterized by a leptokurtic behavior. Consequently, the Bayesian credible intervals (Table 5) for the SHPs are extremely narrow, thus indicating their good identifiability. The Bayesian analysis reveals, as expected, a

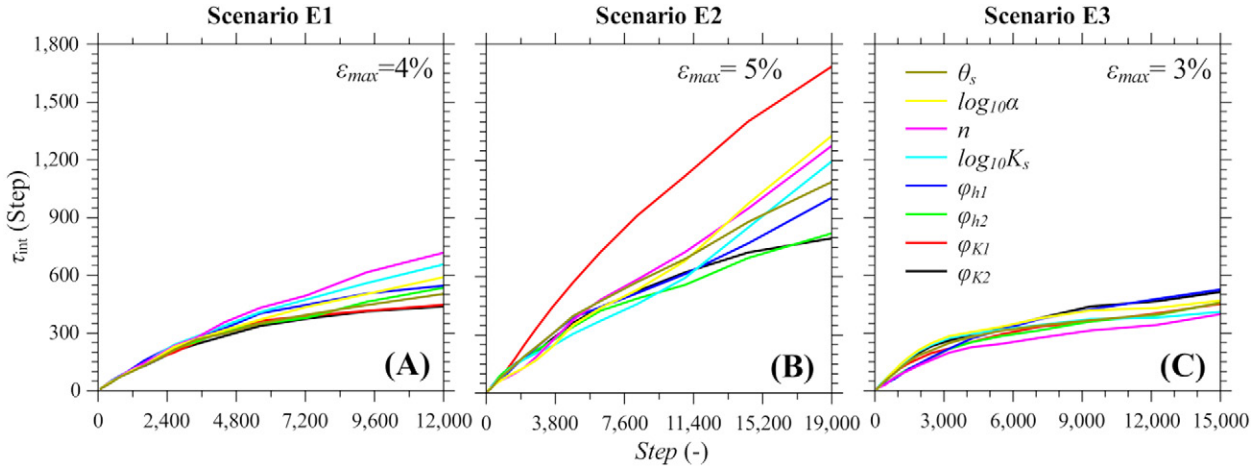

Fig. 7. The diagnostic plot of the Affine Invariant Ensemble Sampler (AIES) algorithm for the experimental data analysis scenario showing the integrated autocorrelation time τ_{int} against the algorithm step for the soil hydraulic parameters of residual soil water content (θ_r), saturated soil water content (θ_s), the van Genuchten–Mualem parameters n and α, saturated hydraulic conductivity (K_s), and scaling factors for hydraulic head and hydraulic conductivity (φ_{h1} and φ_{h2}, and φ_{K1} and φ_{K2} for Soil Materials 1 and 2, respectively), along with the maximum statistical error (ε_{max}) for Scenarios (A) E1, (B) E2, and (C) E3.

well-posed inverse problem characterized by low uncertainty mainly stemming from the simultaneous use of measured water contents at different depths, which better constrains the inverse estimation problem. Overall, the results agree well with those reported by Qu et al. (2016), where the ROSETTA pedotransfer function was used to predict the spatial distribution of SHPs using the soil textural information for the top 5 cm of soil. Indeed, the saturated water content for Soil Material 1 ranges between 0.50 and 0.52 $cm^3\ cm^{-3}$, which is in line with the values of the porosity reported by Qu et al. (2016), ranging between 0.46 and 0.56 $cm^3\ cm^{-3}$ for the southern part of the Rollesbroich catchment. Results slightly deviate for the VGM shape parameters α and n, which are estimated to be higher and lower, respectively, than those of Qu et al. (2016), who reported α and n values ranging between −2.40 and −2.30 cm^{-1} and between 1.63 and 2.23, respectively. Higher uncertainty is found for the saturated hydraulic conductivity of Soil Material 1, which ranges between 10 and 40 cm d^{-1}. It is worth noting that estimates of SHPs using PTFs are usually associated with significant uncertainty. Thus, it is preferable to use inversely estimated SHPs when the model inversion is well posed and the associated uncertainty is properly assessed.

The effect of the parameter uncertainty on the simulated water contents and neutron fluxes is shown in Fig. 9, which reports the model predictive uncertainty (gray lines) obtained by random sampling of 500 solutions from the posterior distribution. The model can accurately describe the soil moisture dynamics in the three observation depths with limited uncertainty. The quality of the fitting is significantly better than that reported by Qu et al. (2014), who inversely estimated the SHPs from soil water contents measured with a sensor network at 41 locations in the Rollesbroich catchment. This error reduction confirms that the use of the scaling factors is a valid approach for this dataset because it results in a better description of water flow than the assumption of homogeneous soil used by Qu et al. (2014). On the other hand, the comparison between simulated and measured aboveground neutron fluxes (Fig. 9A) reveals an appreciable deviation. More specifically, the coupled model tends to overestimate the variability of neutron fluxes. This is particularly evident during August and September 2012. The Rollesbroich site is managed grassland with a relatively low biomass. Except for an occasional snow cover during the winter period, there are no additional transient hydrogen pools that have a strong influence on the measured neutron signal. As a consequence, such behavior can be partially explained by the simplifying assumptions of the COSMIC model, by an imperfect neutron flux correction (e.g., for variations due to fluctuations in the atmospheric density and humidity or incoming neutrons), and by an inadequate calibration of the COSMIC model parameters. In such circumstances, two approaches can be recommended:

1. Two-Step Sequential Calibration: First, the HYDRUS model is preliminarily calibrated against measured data from different locations and depths in the measurement footprint of the cosmic-ray probe. Next, the calibrated HYDRUS model is coupled with the COSMIC model for the inverse estimation of the COSMIC parameters from the measured neutron fluxes. It must be emphasized that the possibility of using simulated high-resolution soil moisture profiles instead of a few point measurements at different soil depths can increase the accuracy of the COSMIC model predictions. In this perspective, it may be worth coupling the three-dimensional model (e.g., HYDRUS 2D/3D), with the COSMIC model to account for the horizontal and vertical soil heterogeneity at the field scale (≈300 m). The recent work of Gibson and Franz (2018) suggested that sparse point measurements of the SHPs can significantly improve the description of spatial patterns of SHPs.
2. Joint Calibration: The soil hydraulic and COSMIC parameters are jointly estimated using the coupled HYDRUS–COSMIC

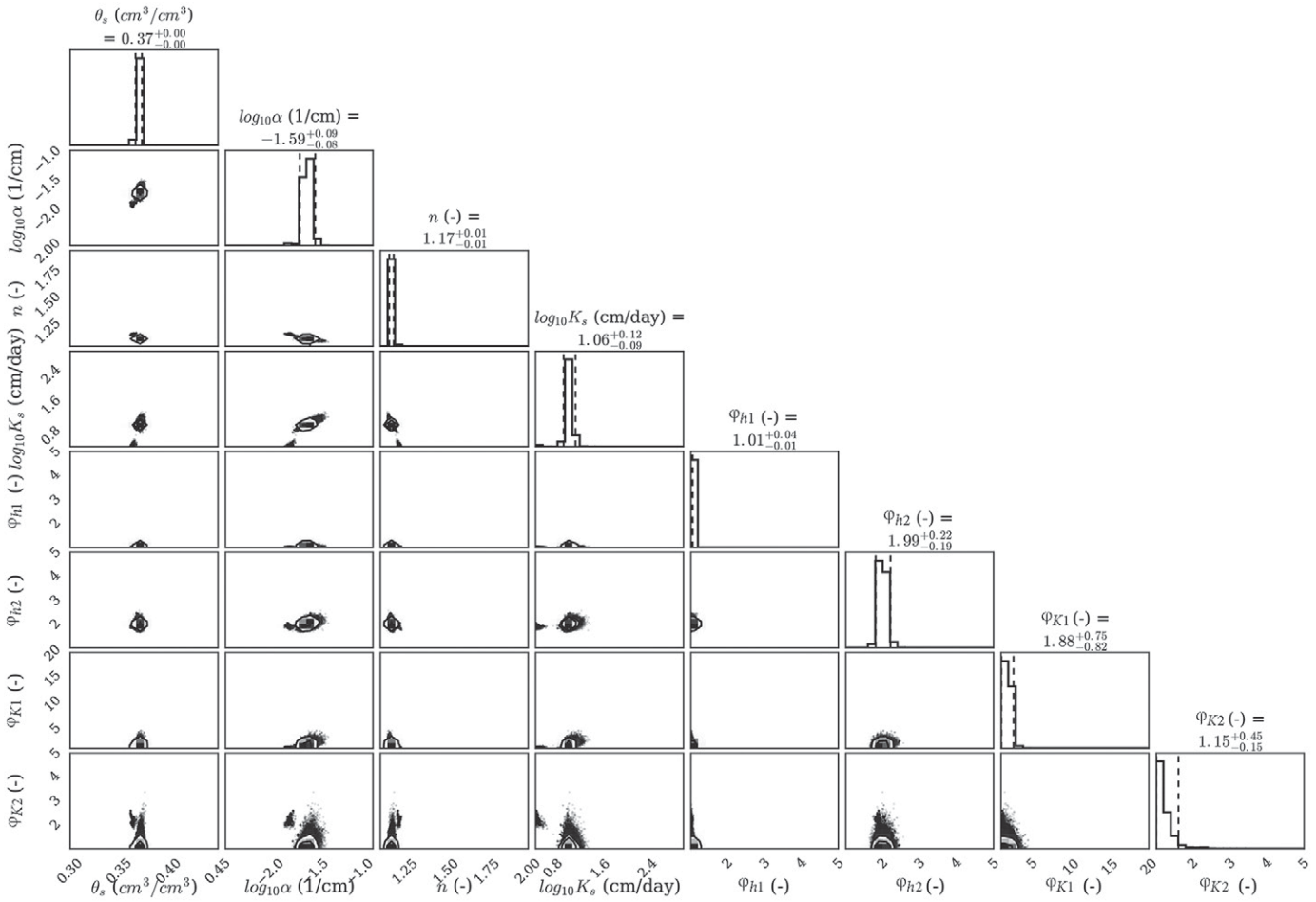

Fig. 8. Joint (below diagonal) and marginal (diagonal) posterior distributions of the soil hydraulic parameters of saturated soil water content (θ_s), the van Genuchten–Mualem parameters n and α, saturated hydraulic conductivity (K_s), and scaling factors for hydraulic head and hydraulic conductivity (φ_{h1} and φ_{h2}, and φ_{K1} and φ_{K2} for Soil Materials 1 and 2, respectively) for Scenario E3. The isolines and the dashed lines indicate the 12, 39, 68, and 84% probability levels and the Bayesian credible intervals, respectively. The axis ranges correspond to the parameter bounds reported in Table 3.

model using both measured neutron fluxes and volumetric water contents. However, this will increase the dimensionality of the inverse problem, which can lead to convergence issues in the MCMC analysis.

The joint and marginal posterior distributions of the soil hydraulic parameters for Scenario E1 that relies on measured aboveground neutron flux are shown in Fig. 10. It is evident that the measured neutron fluxes do not provide sufficient information to update the prior distributions of φ_{h2}, φ_{K1}, and φ_{K2}, which remain almost flat after the MCMC analysis. Indeed, their Bayesian credible intervals (Table 5) are only marginally narrower than the prior bounds listed in Table 3. A similar but less pronounced behavior is visible for K_s and φ_{h1}, although the marginal posterior distributions are right skewed, thus indicating a slight influence of the measured data on these parameters. It is worth noting that the MCMC analysis reveals a highly skewed bivariate posterior distribution for the pair of parameters α–K_s. In such circumstances, the affine invariant properties of the AIES algorithm significantly mitigate convergence issues usually encountered in traditional MCMC algorithms.

Interestingly, the use of measured neutron fluxes leads to well-constrained estimates of VGM shape parameters, thus confirming the findings of the synthetic modeling scenarios. The confident estimation of θ_s stems from the use of near-saturated water contents, which better constrain the inverse problem. This effect is more pronounced for n and θ_s, while α presents a more platykurtic distribution. In particular, the Bayesian credible intervals for θ_s and n range between 0.33 and 0.38 $cm^3\ cm^{-3}$ and between 1.10 and 1.47, respectively, which are slightly larger than those obtained in Scenario E3. On the other hand, α ranges between 0.004 and 0.04 cm^{-1}, thus indicating a tendency to overestimate the soil water retention capacity. Indeed, very low values of α are usually associated with a high retention capacity and delayed desaturation of the porous medium. In such circumstances, simulated water content fluctuations are limited and propagated in the calculation of the fast neutron fluxes. Thus, from a numerical point of view, the Bayesian inference process adjusted the SHPs to compensate for other plausible sources of uncertainty (e.g., COSMIC model assumptions, COSMIC parameters). Therefore, the results for Scenario E1 further confirm the findings for Scenario E3 and

suggest the use of a joint Bayesian calibration of the HYDRUS–COSMIC model.

This aspect is further investigated in Fig. 11, which shows a comparison between measured (black circles) and modeled depth-weighted soil water contents. In particular, measured data are compared with soil water contents calculated from the CRNP using the standard calibration method (Baatz et al., 2014) (a gray line in Fig. 11) and predicted using the model with the median SHPs from the posterior distribution for Scenario E1 (a black line in Fig. 11), respectively. Depth-weighted soil water contents are obtained using weights of 0.852, 0.146, and 0.002 at $z = -5$, -20, and -50 cm, respectively, as reported by Baatz et al. (2014). Overall, both methods provide a good description of the near-surface soil water contents as indicated by low RMSE values. An appreciable overestimation of the water content can be observed for both methods between August and September 2012, with the magnitude being higher for the COSMIC-predicted water contents (a black line in Fig. 11), which generally exhibit a lower variability than water contents calculated using the standard calibration method. Such difference confirms potential approximations in the COSMIC modeling assumptions and an imperfect calibration of the COSMIC parameters, although deviation from the measured data is limited.

Figure 12 shows the model predictive uncertainty (gray lines) in the simulated neutron fluxes (Fig. 12A) and volumetric water contents at three different depths. It is evident that both the discrepancy between measurement and model and the uncertainty grow with depth. The model predictive uncertainty only partially encompasses the measured data, and the water contents are considerably underestimated at $z = -50$ cm. This behavior is expected because the measured neutron fluxes are mostly informative of near-surface water dynamics. Furthermore, the results indicate that the variability of water content is underestimated. This is particularly visible between June and September 2012 at $z = -5$ and -20 cm, and it can be partially explained by the previously described underestimation of the shape parameter α.

Table 5. 95% Bayesian credible intervals of the soil hydraulic parameters for the three experimental scenarios. The 2.5 and 97.5% quantiles are the bounds of the credible intervals.

	Scenario					
	E1		E2		E3	
Parameter†	2.5%	97.5%	2.5%	97.5%	2.5%	97.5%
θ_s, cm^3 cm^{-3}	0.33	0.38	0.35	0.39	0.36	0.37
$\log_{10}\alpha$, cm^{-1}	−2.40	−1.41	−1.87	−0.93	−1.67	−1.49
n	1.10	1.47	1.14	1.24	1.15	1.18
$\log_{10}K_s$, cm d^{-1}	0.50	2.82	0.50	1.44	0.97	1.18
φ_{h1}	1.00	4.32	1.00	2.33	1.00	1.05
φ_{h2}	1.27	5.00	1.00	4.35	1.80	2.21
φ_{K1}	1.00	18.94	1.00	11.51	1.07	2.63
φ_{K2}	1.00	4.78	1.00	4.65	1.00	1.60

† θ_s, saturated water content; α and n, shape parameters; K_s, saturated hydraulic conductivity, φ_{h1} and φ_{K1}, and φ_{h2} and φ_{K2}, pressure head and saturated hydraulic conductivity scaling factors for Soil Materials 1 and 2, respectively.

Overall, this analysis suggests that CRNP data can provide reasonable estimates of the effective SHPs at the field scale, which can be extremely valuable in land surface hydrological modeling. In particular, the VGM shape parameters and the saturated water content are successfully inferred from the measured neutron flux, thus leading to a coherent simulation of the soil moisture dynamics in the near surface, which is crucial for a proper description of the surface energy balance in LSMs (Iwema et al., 2017). The large uncertainty observed for K_s can significantly affect simulations of overland flow and the partitioning of precipitation into infiltration and surface runoff, and thus other types of measurements are needed to better constrain this parameter. Nevertheless, the large footprint of CRNPs represents an important advantage compared with classical near-surface point measurements, the information content of which can be affected by various sources of uncertainty. This aspect is better investigated in the final experimental data analysis scenario.

Figure 13 shows the joint and marginal posterior distributions for Scenario E2 that relies on near-surface water content measurements only. A multimodal posterior distribution with two peaks is observed for both α and K_s. The examination of the joint posterior distribution of the pair α–K_s reveals the existence of two regions of high probability, one centered around the location [$\log_{10}\alpha = -1.7$, $\log_{10}K_s = 0.5$] and another one around [$\log_{10}\alpha = -1.2$, $\log_{10}K_s = 1.3$]. While the first region of high probability is in line with the values obtained for Scenarios E1 and E3 and thus probably reflects the true SHPs, the latter first region of high probability significantly overestimates the shape parameter α. Such predictions could be representative of another plausible pore system induced by the plowing of the top layer. These sources of uncertainty propagate in the credible interval (Table 5), which now ranges between 0.01 and 0.11 cm^{-1}, thus indicating poor identifiability of the α parameter. In this view, it must be emphasized that aboveground neutron fluxes are less influenced by local sources of uncertainty than near-surface point measurements due to their footprint and penetration depth.

On the other hand, θ_s and n are well constrained and in line with the values obtained in the previous two scenarios. A significant uncertainty is noticeable for the scaling factor φ_{K1}, which ranges between 1.0 and 11.51, despite being characterized by an apparently strong unimodal posterior distribution. In particular, a region of high probability is evident around 1.0, followed by a flat valley of low probability. Such posterior distributions are mainly responsible for the large integrated autocorrelation time observed in Fig. 7. Nevertheless, a comparison of the posterior distributions of the scaling factors of Soil Materials 1 and 2 confirms that the measured water contents at $z = -5$ cm are mainly informative of the soil hydraulic properties of the surface layer. Indeed, the posterior distributions of φ_{h2} and φ_{K2} are very similar to the prior distributions, whereas the posterior distributions clearly are much smaller for φ_{h1} and φ_{K1}.

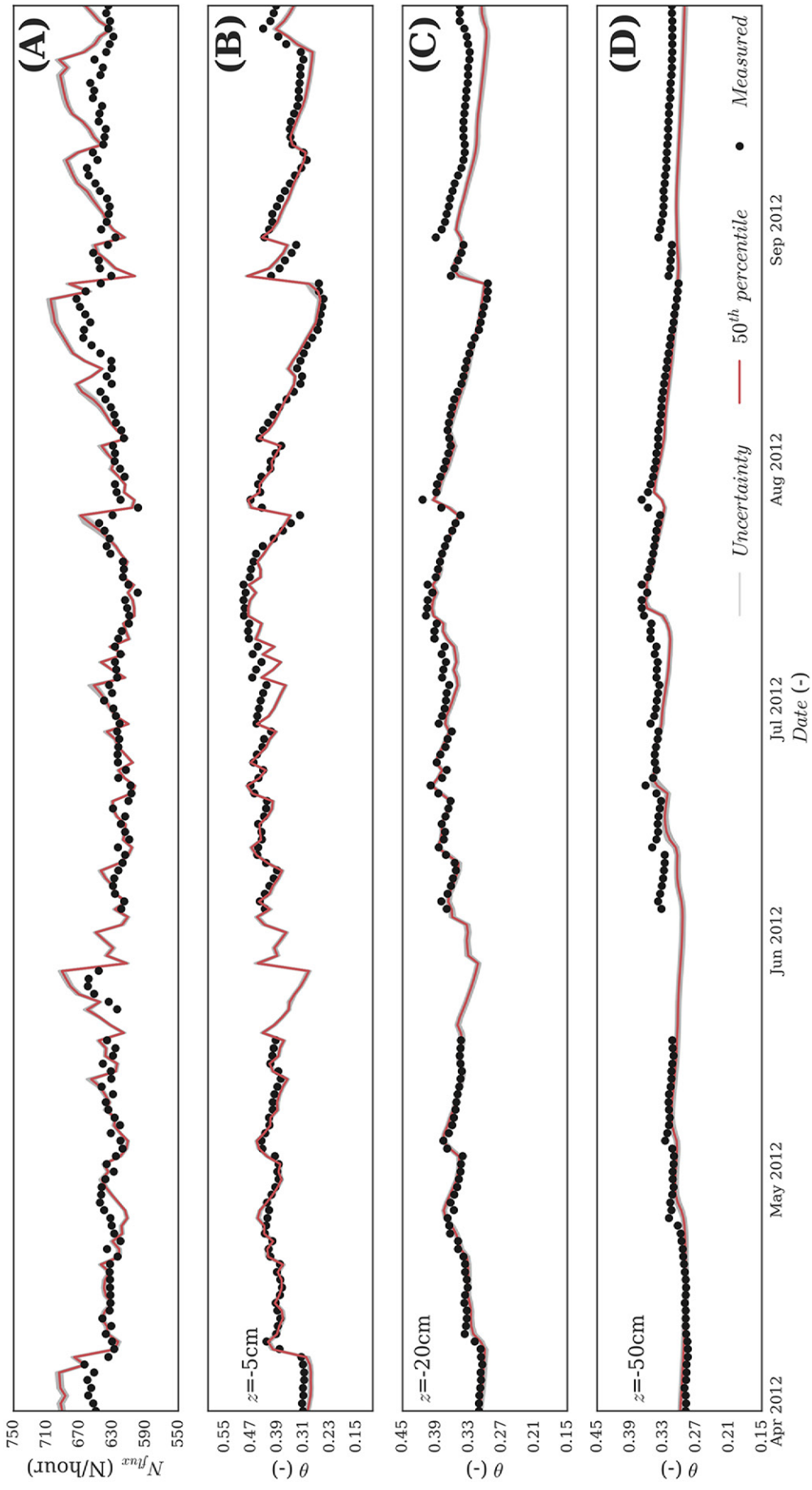

Fig. 9. A comparison between the model predictions (gray lines) obtained by random sampling of 500 solutions from the posterior distribution (Scenario E3) and measured (black circles) (A) neutron fluxes (N_{flux}) and (B,C,D) volumetric water contents (θ) at three different depths. The red lines indicate the model prediction with the median soil hydraulic parameters from the posterior distribution.

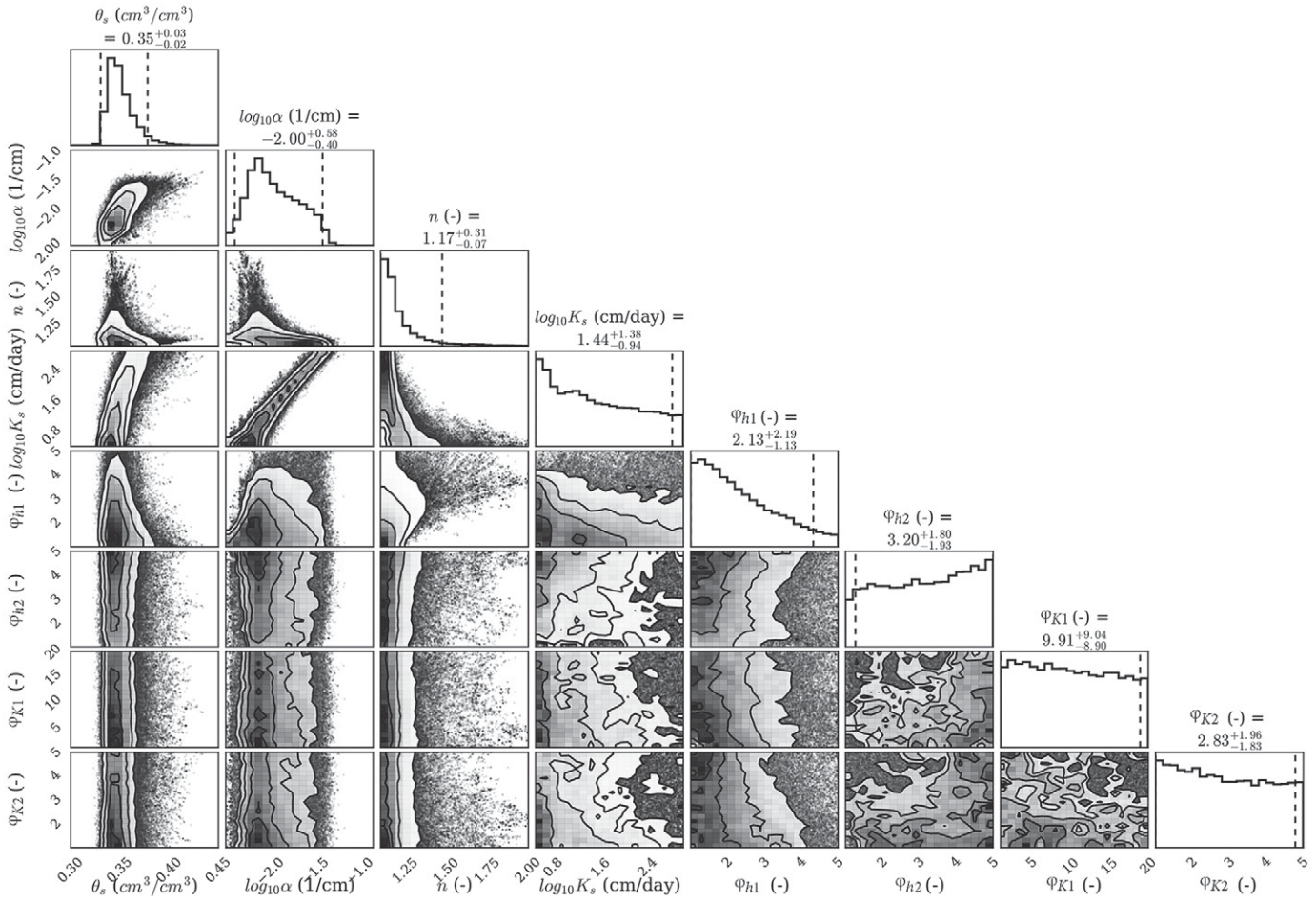

Fig. 10. Joint (below diagonal) and marginal (diagonal) posterior distributions of the soil hydraulic parameters of saturated soil water content (θ_s), the van Genuchten–Mualem parameters n and α, saturated hydraulic conductivity (K_s), and scaling factors for hydraulic head and hydraulic conductivity (φ_{h1} and φ_{h2}, and φ_{K1} and φ_{K2} for Soil Materials 1 and 2, respectively) for Scenario E1. The isolines and the dashed lines indicate the 12, 39, 68, and 84% probability levels and the Bayesian credible intervals, respectively. The axis ranges correspond to the parameter bounds reported in Table 3.

The propagation of uncertainty in the model predictions for Scenario E2 is shown in Fig. 14. It is again evident that the underestimation of the soil retention capacity, caused by the low inferred values of the shape parameter α, results in lower values of the water contents at $z = -20$ and -50 cm. The reduced retention capacity propagates in the simulated aboveground neutron fluxes, which are significantly overestimated. However, the magnitude of the uncertainty is smaller than that obtained for the water contents at deeper soil horizons, which is expected because neutron fluxes are mostly influenced by the soil moisture dynamics in the near surface.

As a result of these analyses, a number of conclusions can be drawn:

- The results for Scenario E3 indicate that it is not possible to simultaneously fit the measured neutron flux and soil water content data. This may be related to uncorrected effects of aboveground biomass on the measured neutron data or inadequate modeling assumptions. In particular, the deviation

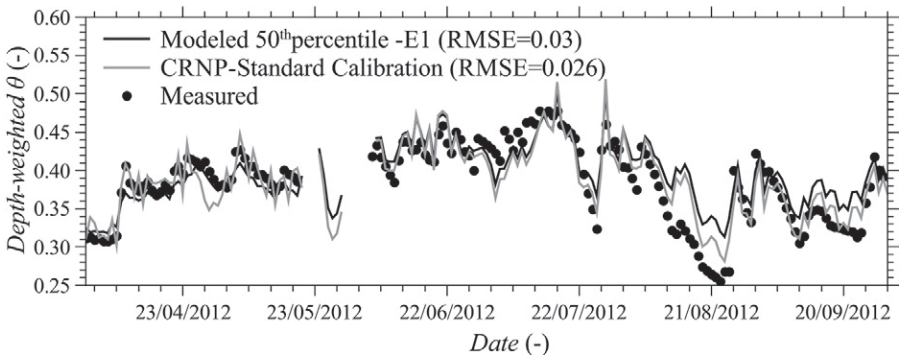

Fig. 11. A comparison between measured (black circles) and modeled (solid lines) depth-weighted soil water contents (θ). The gray and black lines indicate soil water contents calculated from the cosmic-ray neutron probes (CRNP) using the standard calibration method (Baatz et al., 2014) and predicted using the model with the median soil hydraulic parameters from the posterior distribution from Scenario E1, respectively.

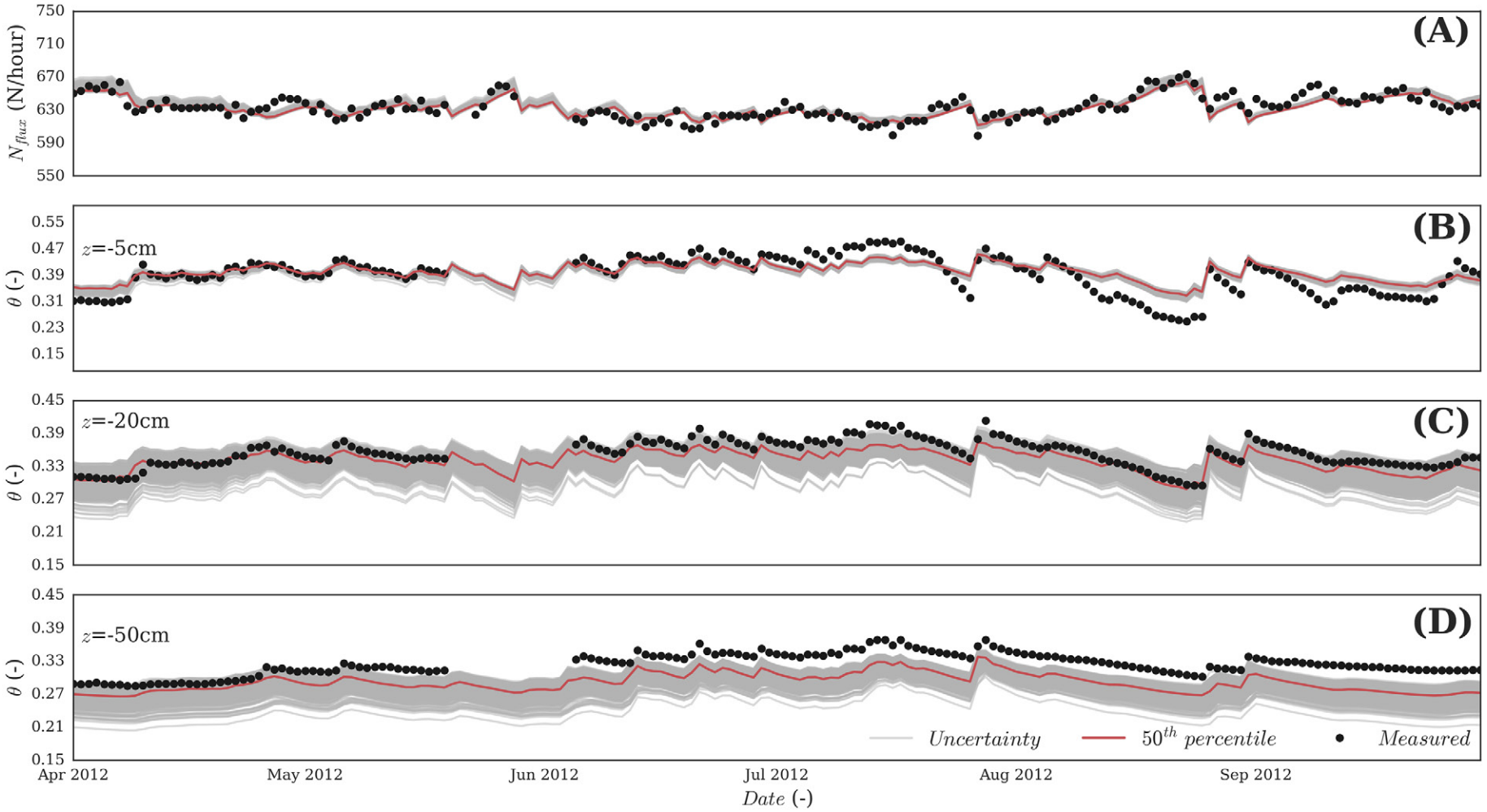

Fig. 12. A comparison between the model predictions (gray lines) obtained by random sampling of 500 solutions from the posterior distribution (Scenario E1) and (A) measured (black circles) neutron fluxes (N_{fluxes}) and (B,C,D) volumetric water contents (θ) at three different depths. The red lines indicate the model prediction with the median soil hydraulic parameters from the posterior distribution.

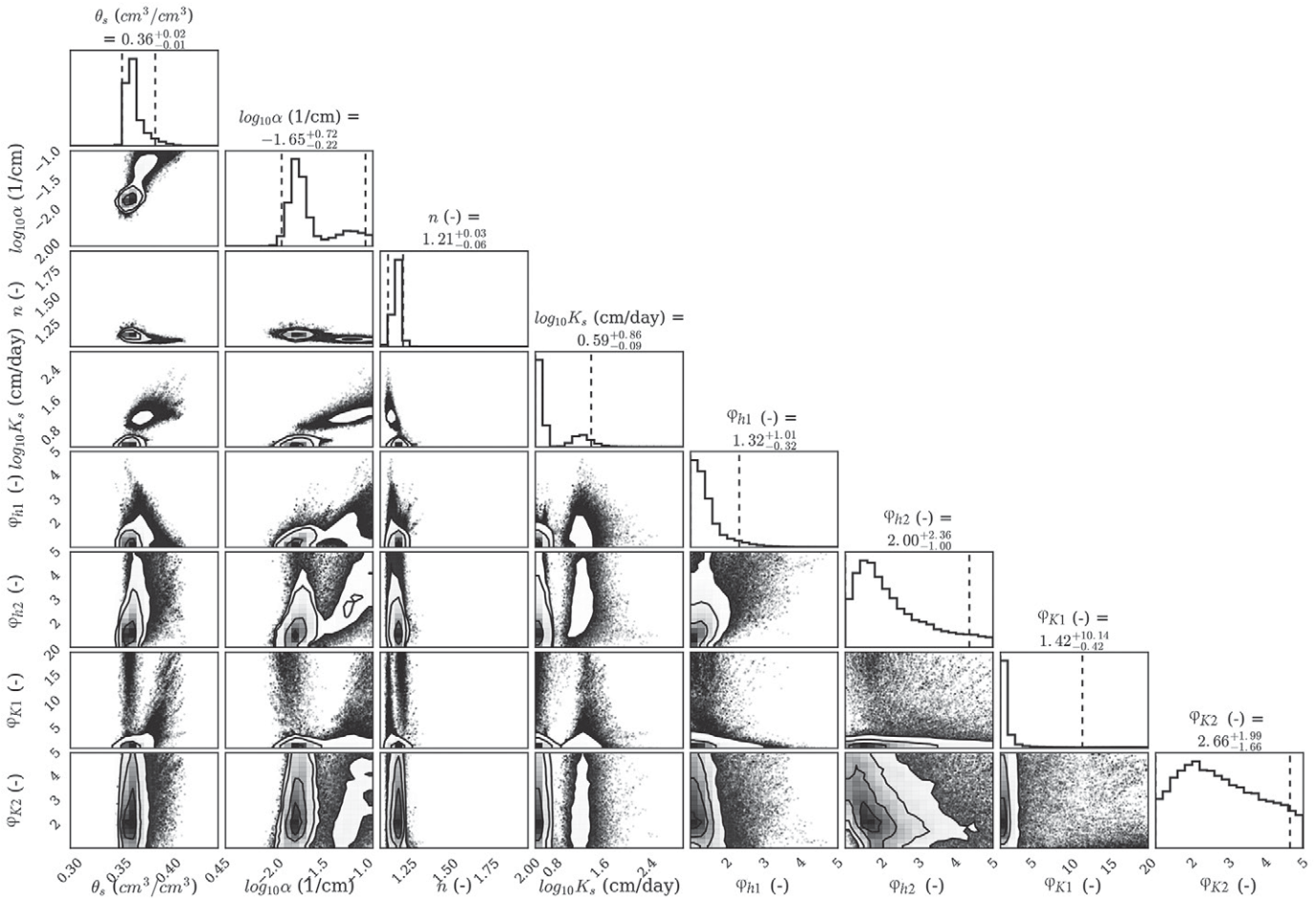

Fig. 13. Joint (below diagonal) and marginal (diagonal) posterior distributions of the soil hydraulic parameters of saturated soil water content (θ_s), the van Genuchten–Mualem parameters n and α, saturated hydraulic conductivity (K_s), and scaling factors for hydraulic head and hydraulic conductivity (φ_{h1} and φ_{h2}, and φ_{K1} and φ_{K2} for Soil Materials 1 and 2, respectively) for Scenario E2. The isolines and the dashed lines indicate the 12, 39, 68, and 84% probability levels and the Bayesian credible intervals, respectively. The axis ranges correspond to the parameter bounds reported in Table 3.

between measured neutron fluxes and those simulated by the calibrated HYDRUS model suggest potential inaccuracies in the COSMIC parameters. This could potentially be addressed with a two-step sequential or a joint calibration of the coupled HYDRUS–COSMIC model.

- The use of measured aboveground neutron fluxes led to a reasonably confident estimation of the VGM shape parameters and the saturated water content. From this point of view, the possibility of inversely estimating the effective soil hydraulic parameters at the field scale from the CRNP data is confirmed. The combination of neutron data with other independent types of measurements (e.g., soil porosity, saturated conductivity) can further reduce the parameter uncertainty.
- A comparison of inversion results obtained for near-surface volumetric water contents or neutron fluxes revealed that the latter are less influenced by typical sources of uncertainty associated with land surface management activities (e.g., soil tillage), thus leading to more reliable and representative estimates of soil hydraulic parameters.

Conclusions and Summary

The main goal of this study was to assess the information content of cosmic-ray neutron data for the inverse estimation of the effective soil hydraulic parameters. An extensive theoretical and experimental assessment based on the combination of the coupled HYDRUS–COSMIC model with a Bayesian data analysis framework revealed that neutron fluxes could be used effectively to estimate the SHPs. In particular, the analysis of both synthetic and actual data from homogeneous and heterogeneous soil profiles led to a confident estimation of the VGM shape parameters. Moreover, the analysis demonstrated that the residual and saturated water contents can be successfully inferred from measured neutron fluxes if the soil approximately reaches a dry or wet state, respectively. On the other hand, high uncertainty was observed for the saturated hydraulic conductivity, which suggests that the joint consideration of CRNP data with independent measurements of this parameter may be required. The simultaneous use of both neutron flux and water content data resulted in an appreciable reduction in uncertainty, in particular for the VGM shape parameters and

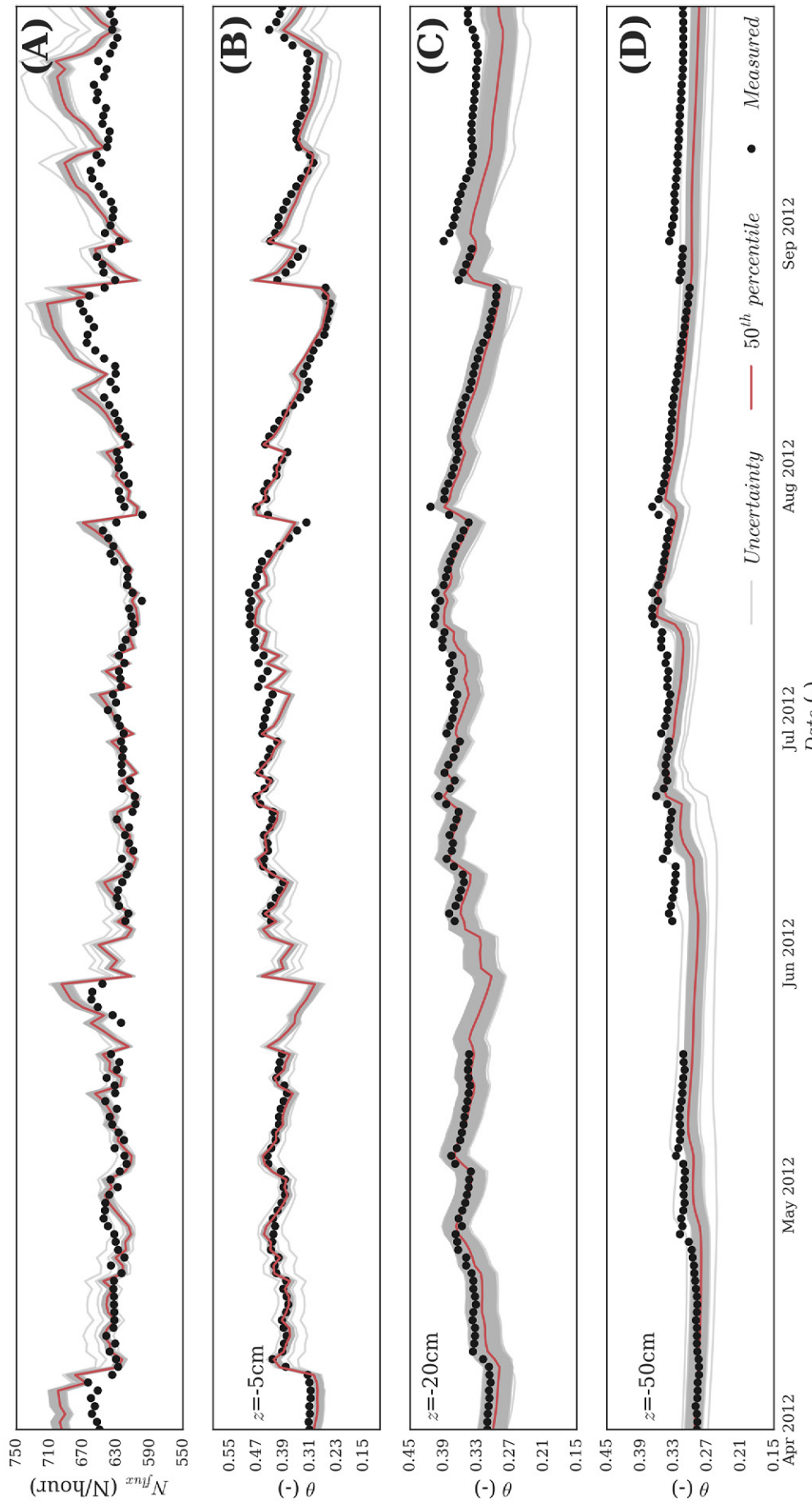

Fig. 14. A comparison between the model predictions (gray lines) obtained by random sampling of 500 solutions from the posterior distribution (Scenario E2) and (A) measured (black circles) neutron fluxes (N_{fluxes}) and (B,C,D) volumetric water contents (θ) at three different depths. The red lines indicate the model prediction with the median soil hydraulic parameters from the posterior distribution.

for the saturated hydraulic conductivity. This result opens new perspectives to estimate soil hydraulic properties from the combination of CRNP and other remote sensing techniques. However, to have a precise assessment of the benefits of such joint inversion for LSMs, it is worth investigating numerically the propagation of the uncertainty in values of SHPs using LSMs. In this perspective, a model-based Bayesian experimental design could be used to optimize the location and the number of cosmic-ray probes and traditional sensors to minimize the effect of the uncertainty on the land surface processes analyzed.

Furthermore, the comparison between the results obtained with the use of traditional near-surface point measurements and CRNP data indicates that the latter data are less influenced by the typical sources of uncertainty induced by land surface management activities (e.g., plowing) and lead to a more representative estimation of the soil hydraulic parameters, which is fundamental when dealing with land surface hydrological modeling. In particular, the shape parameter α, which characterizes the soil retention capacity, was significantly overestimated when inversions were solely based on near-surface water content measurements, leading to a bimodal posterior distribution representative of another plausible pore system induced by former land management activities and macropores. On the other hand, the CRNP penetration depth and footprint significantly mitigate these issues. Nevertheless, to what extent this difference in the estimation of the SHPs is significant for practical purposes depends on the type of analysis performed by the modeler (e.g., surface runoff, infiltration, solute fluxes) and can be clarified only by propagating the estimated uncertainty. In this perspective, further studies are encouraged to better assess the information content gain of CRNP data in hydrological modeling.

In addition, the analysis presented here suggests that the coupled HYDRUS–COSMIC model can be used to detect and correct an imperfect calibration of the COSMIC parameters. Avery et al. (2016) provided extensive results about the correlation between lattice water and the soil clay fraction. The relationship reported in this study can be used to better constrain COSMIC parameters. Moreover, future research should consider the coupling of the COSMIC model with HYDRUS-3D to better account for horizontal and vertical soil heterogeneity at the field scale. In this perspective, the use of CRNP rover data could improve the description of the spatial patterns of SHPs (Gibson and Franz, 2018). A computationally cheap alternative would be to use the kriging technique (Brunetti et al., 2017) to interpolate the HYDRUS-1D predictions.

Acknowledgments

We thank the TERENO (Terrestrial Environmental Observatories) project funded by the Helmholtz Association and the Transregional Collaborative Research Center 32 "Patterns in Soil–Vegetation–Atmosphere Systems" funded by Deutsche Forschungsgemeinschaft (DFG) for providing data for this study.

References

Allen, R.G., L.S. Pereira, D. Raes, and M. Smith. 1998. Crop evapotranspiration. Irrig. Drain. Pap. 56. FAO, Rome. doi:10.1016/j.eja.2010.12.001

Andreasen, M., K.H. Jensen, D. Desilets, T.E. Franz, M. Zreda, H.R. Bogena, and M.C. Looms. 2017. Status and perspectives on the cosmic-ray neutron method for soil moisture estimation and other environmental science applications. Vadose Zone J. 16(8). doi:10.2136/vzj2017.04.0086

Avery, W.A., C. Finkenbiner, T.E. Franz, T. Wang, A.L. Nguy-Robertson, A. Suyker, et al. 2016. Incorporation of globally available datasets into the roving cosmic-ray neutron probe method for estimating field-scale soil water content. Hydrol. Earth Syst. Sci. 20:3859–3872. doi:10.5194/hess-20-3859-2016

Baatz, R., H.R. Bogena, H.J. Hendricks Franssen, J.A. Huisman, W. Qu, C. Montzka, and H. Vereecken. 2014. Calibration of a catchment scale cosmic-ray probe network: A comparison of three parameterization methods. J. Hydrol. 516:231–244. doi:10.1016/j.jhydrol.2014.02.026

Baatz, R., H.J.H. Franssen, X. Han, T. Hoar, H.R. Bogena, and H. Vereecken. 2017. Evaluation of a cosmic-ray neutron sensor network for improved land surface model prediction. Hydrol. Earth Syst. Sci. 21:2509–2530. doi:10.5194/hess-21-2509-2017

Betancourt, M. 2017. A conceptual introduction to Hamiltonian Monte Carlo. https://arxiv.org/pdf/1701.02434.pdf.

Beven, K., and A. Binley. 1992. The future of distributed models: Model calibration and uncertainty prediction. Hydrol. Processes 6:279–298. doi:10.1002/hyp.3360060305

Bogena, H.R., M. Herbst, J.A. Huisman, U. Rosenbaum, A. Weuthen, and H. Vereecken. 2010. Potential of wireless sensor networks for measuring soil water content variability. Vadose Zone J. 9:1002–1013. doi:10.2136/vzj2009.0173

Bogena, H.R., J.A. Huisman, A. Güntner, C. Hübner, J. Kusche, F. Jonard, et al. 2015. Emerging methods for noninvasive sensing of soil moisture dynamics from field to catchment scale: A review. Wiley Interdiscip. Rev. Water 2:635–647. doi:10.1002/wat2.1097

Bogena, H.R., J.A. Huisman, B. Schilling, A. Weuthen, and H. Vereecken. 2017. Effective calibration of low-cost soil water content sensors. Sensors 17:208. doi:10.3390/s17010208

Bogena, H.R., R. Kunkel, S. Zacharias, T. Pütz, M. Schwank, O. Bens, et al. 2012. TERENO: Long-term monitoring network for terrestrial research. Hydrol. Wasserbewirtsch. 56:138–143.

Bogena, H.R., C. Montzka, J.A. Huisman, A. Graf, M. Schmidt, M. Stockinger, et al. 2018. The TERENO-Rur Hydrological Observatory: A multi-scale multi-compartment research platform for the advancement of hydrological science. Vadose Zone J. 17:180055. doi:10.2136/vzj2018.03.0055

Brunetti, G., J. Šimůnek, and P. Piro. 2016. A comprehensive numerical analysis of the hydraulic behavior of a permeable pavement. J. Hydrol. 540:1146–1161. doi:10.1016/j.jhydrol.2016.07.030

Brunetti, G., J. Šimůnek, M. Turco, and P. Piro. 2017. On the use of surrogate-based modeling for the numerical analysis of low impact development techniques. J. Hydrol. 548:263–277. doi:10.1016/j.jhydrol.2017.03.013

Carsel, R.F., and R.S. Parrish. 1988. Developing joint probability distributions of soil water retention characteristics. Water Resour. Res. 24:755–769 doi:10.1029/WR024i005p00755

Dane, J.H., and S. Hruska. 1983. In-situ determination of soil hydraulic properties during drainage. Soil Sci. Soc. Am. J. 47:619–624. doi:10.2136/sssaj1983.03615995004700040001x

Deng, H., M. Ye, M.G. Schaap, and R. Khaleel. 2009. Quantification of uncertainty in pedotransfer function-based parameter estimation for unsaturated flow modeling. Water Resour. Res. 45:W04409. doi:10.1029/2008WR007477

Desilets, D., M. Zreda, and T.P.A. Ferré. 2010. Nature's neutron probe: Land surface hydrology at an elusive scale with cosmic rays. Water Resour. Res. 46:W11505. doi:10.1029/2009WR008726

Ek, M.B., K.E. Mitchell, Y. Lin, E. Rogers, P. Grunmann, V. Koren, et al. 2003. Implementation of Noah land surface model advances in the National Centers for Environmental Prediction operational mesoscale Eta model. J. Geophys. Res. 108:8851. doi:10.1029/2002JD003296

Evans, J.G., H.C. Ward, J.R. Blake, E.J. Hewitt, R. Morrison, M. Fry, et al. 2016. Soil water content in southern England derived from a cosmic-ray soil moisture observing system: COSMOS-UK. Hydrol. Process. 30:4987–4999. doi:10.1002/hyp.10929

Feddes, R.A., P.J. Kowalik, and H. Zaradny. 1978. Simulation of field water

use and crop yield. PUDOC, Wageningen, the Netherlands.

Feroz, F., M.P. Hobson, and M. Bridges. 2009. MultiNest: An efficient and robust Bayesian inference tool for cosmology and particle physics. Mon. Not. R. Astron. Soc. 398:1601–1614. doi:10.1111/j.1365-2966.2009.14548.x

Finkenbiner, C.E., T.E. Franz, J. Gibson, D.M. Heeren, and J. Luck. 2018. Integration of hydrogeophysical datasets and empirical orthogonal functions for improved irrigation water management. Precis. Agric. (in press). doi:10.1007/s11119-018-9582-5

Foreman-Mackey, D., D.W. Hogg, D. Lang, and J. Goodman. 2012. emcee: The MCMC hammer. Publ. Astron. Soc. Pac. 125:306–312. doi:10.1086/670067

Franz, T.E., M. Zreda, T.P.A. Ferre, R. Rosolem, C. Zweck, S. Stillman, X. Zeng, and W.J. Shuttleworth. 2012. Measurement depth of the cosmic ray soil moisture probe affected by hydrogen from various sources. Water Resour. Res. 48:W08515. doi:10.1029/2012WR011871

Gibson, J., and T.E. Franz. 2018. Spatial prediction of near surface soil water retention functions using hydrogeophysics and empirical orthogonal functions. J. Hydrol. 561:372–383. doi:10.1016/j.jhydrol.2018.03.046

Goodman, J., and J. Weare. 2010. Ensemble samplers with affine invariance. Comm. App. Math. Comp. Sci. 5:65–80. doi:10.2140/camcos.2010.5.65

Gutmann, E.D., and E.E. Small. 2007. A comparison of land surface model soil hydraulic properties estimated by inverse modeling and pedotransfer functions. Water Resour. Res. 43:W05418. doi:10.1029/2006WR005135

Hawdon, A., D. McJannet, and J. Wallace. 2014. Calibration and correction procedures for cosmic-ray neutron soil moisture probes located across Australia. Water Resour. Res. 50:5029–5043. doi:10.1002/2013WR015138

Hopmans, J.W., D.R. Nielsen, and K.L. Bristow. 2002. How useful are small-scale soil hydraulic property measurements for large-scale vadose zone modeling? In P.A.C. Raats et al., editor, Environmental mechanics: Water, mass and energy transfer in the biosphere. Geophys. Monogr. Ser. 129. Am. Geophys. Union, Washington, DC. p. 247–258. doi:10.1029/129GM20

Huijser, D., J. Goodman, and B.J. Brewer. 2015. Properties of the affine invariant ensemble sampler in high dimensions. arXiv:1509.02230.

Huisman, J.A., J. Rings, J.A. Vrugt, J. Sorg, and H. Vereecken. 2010. Hydraulic properties of a model dike from coupled Bayesian and multi-criteria hydrogeophysical inversion. J. Hydrol. 380:62–73. doi:10.1016/j.jhydrol.2009.10.023

Iden, S.C., and W. Durner. 2007. Free-form estimation of the unsaturated soil hydraulic properties by inverse modeling using global optimization. Water Resour. Res. 43:W07451. doi:10.1029/2006WR005845

Ines, A.V.M., and B.P. Mohanty. 2008. Near-surface soil moisture assimilation for quantifying effective soil hydraulic properties under different hydroclimatic conditions. Vadose Zone. J. 7:39–52. doi:10.2136/vzj2007.0048

Iwema, J., R. Rosolem, M. Rahman, E. Blyth, and T. Wagener. 2017. Land surface model performance using cosmic-ray and point-scale soil moisture measurements for calibration. Hydrol. Earth Syst. Sci. 21:2843–2861. doi:10.5194/hess-21-2843-2017

Kavetski, D., G. Kuczera, and S.W. Franks. 2006. Bayesian analysis of input uncertainty in hydrological modeling: 1. Theory. Water Resour. Res. 42:W03407. doi:10.1029/2005WR004368

Kennedy, J., and R. Eberhart. 1995. Particle swarm optimization. Eng. Technol. 1942–1948. doi:10.1109/ICNN.1995.488968

Köhli, M., M. Schrön, M. Zreda, U. Schmidt, P. Dietrich, and S. Zacharias. 2015. Footprint characteristics revised for field-scale soil moisture monitoring with cosmic-ray neutrons. Water Resour. Res. 51:5772–5790 . doi:10.1002/2015WR017169

Kool, J.B., and J.C. Parker. 1988. Analysis of the inverse problem for transient unsaturated flow. Water Resour. Res. 24:817–830. doi:10.1029/WR024i006p00817

Lam, S.K., A. Pitrou, and S. Seibert. 2015. Numba: A LLVM-based Python JIT compiler. In: Proceedings of the 2nd Workshop on the LLVM Compiler Infrastructure in HPC, Austin, TX. 15–20 Nov. 2015. Assoc. Comput. Mach., New York. Article no. 7. doi:10.1145/2833157.2833162

Mantovan, P., and E. Todini. 2006. Hydrological forecasting uncertainty assessment: Incoherence of the GLUE methodology. J. Hydrol. 330:368–381. doi:10.1016/j.jhydrol.2006.04.046

Matthews, C., J. Weare, A. Kravtsov, and E. Jennings. 2017. Umbrella sampling: A powerful method to sample tails of distributions. Mon. Not. R. Astron. Soc. 480:4069–4079. doi:10.1093/mnras/sty2140

Metropolis, N., A.W. Rosenbluth, M.N. Rosenbluth, A.H. Teller, and E. Teller. 1953. Equation of state calculations by fast computing machines. J. Chem. Phys. 21:1087–1092. doi:10.1063/1.1699114

Mockler, E.M., K.P. Chun, G. Sapriza-Azuri, M. Bruen, and H.S. Wheater. 2016. Assessing the relative importance of parameter and forcing uncertainty and their interactions in conceptual hydrological model simulations. Adv. Water Resour. 97:299–313. doi:10.1016/j.advwatres.2016.10.008

Mohanty, B.P. 2013. Soil hydraulic property estimation using remote sensing: A review. Vadose Zone J. 12(4). doi:10.2136/vzj2013.06.0100

Mohanty, B.P., M.H. Cosh, V. Lakshmi, and C. Montzka. 2017. Soil moisture remote sensing: State-of-the-science. Vadose Zone J. 16(1). doi:10.2136/vzj2016.10.0105

Montanari, A. 2007. What do we mean by 'uncertainty'? The need for a consistent wording about uncertainty assessment in hydrology. Hydrol. Process. 21:841–845. doi:10.1002/hyp.6623

Pelowitz, D.B. 2011. MCNPX user's manual version 2.7.0. LA-CP-11-00438. Los Alamos Natl. Lab., Los Alamos, NM.

Pitman, A.J. 2003. The evolution of, and revolution in, land surface schemes designed for climate models. Int. J. Climatol. 23:479–510. doi:10.1002/joc.893

Qu, W., H.R. Bogena, J.A. Huisman, G. Martinez, Y.A. Pachepsky, and H. Vereecken. 2014. Effects of soil hydraulic properties on the spatial variability of soil water content: Evidence from sensor network data and inverse modeling. Vadose Zone J. 13(12). doi:10.2136/vzj2014.07.0099

Qu, W., H.R. Bogena, J.A. Huisman, M. Schmidt, R. Kunkel, A. Weuthen, et al. 2016. The integrated water balance and soil data set of the Rollesbroich Hydrological Observatory. Earth Syst. Sci. Data 8:517–529. doi:10.5194/essd-8-517-2016

Ritchie, J.T. 1972. Model for predicting evaporation from a row crop with incomplete cover. Water Resour. Res. 8:1204–1213. doi:10.1029/WR008i005p01204

Rivera Villarreyes, C.A., G. Baroni, and S.E. Oswald. 2014. Inverse modelling of cosmic-ray soil moisture for field-scale soil hydraulic parameters. Eur. J. Soil Sci. 65:876–886. doi:10.1111/ejss.12162

Santanello, J.A., C.D. Peters-Lidard, M.E. Garcia, D.M. Mocko, M.A. Tischler, M.S. Moran, and D.P. Thoma. 2007. Using remotely-sensed estimates of soil moisture to infer soil texture and hydraulic properties across a semi-arid watershed. Remote Sens. Environ. 110:79–97. doi:10.1016/j.rse.2007.02.007

Schaap, M.G., F.J. Leij, and M.Th. van Genuchten. 2001. Rosetta: A computer program for estimating soil hydraulic parameters with hierarchical pedotransfer functions. J. Hydrol. 251:163–176. doi:10.1016/S0022-1694(01)00466-8

Scharnagl, B., J.A. Vrugt, H. Vereecken, and M. Herbst. 2011. Inverse modelling of in situ soil water dynamics: Investigating the effect of different prior distributions of the soil hydraulic parameters. Hydrol. Earth Syst. Sci. 15:3043–3059. doi:10.5194/hess-15-3043-2011

Schrön, M., M. Köhli, L. Scheiffele, J. Iwema, H.R. Bogena, L. Lv, et al. 2017. Improving calibration and validation of cosmic-ray neutron sensors in the light of spatial sensitivity. Hydrol. Earth Syst. Sci. 21:5009–5030. doi:10.5194/hess-21-5009-2017

Shuttleworth, J., R. Rosolem, M. Zreda, and T. Franz. 2013. The COsmic-ray Soil Moisture Interaction Code (COSMIC) for use in data assimilation. Hydrol. Earth Syst. Sci. 17:3205–3217. doi:10.5194/hess-17-3205-2013

Šimůnek, J., and M.Th. van Genuchten. 1996. Estimating unsaturated soil hydraulic properties from tension disc infiltrometer data by numerical inversion. Water Resour. Res. 32:2683–2696. doi:10.1029/96WR01525

Šimůnek, J., M.Th. van Genuchten, and M. Šejna. 2016. Recent developments and applications of the HYDRUS computer software packages. Vadose Zone J. 15(7). doi:10.2136/vzj2016.04.0033

Sokal, A.D. 1996. Monte Carlo methods in statistical mechanics: Foundations and new algorithms. NATO ASI Ser., Ser. B 361:131–192. doi:10.1007/978-1-4899-0319-8_6

Steenpass, C., J. Vanderborght, M. Herbst, J. Šimůnek, and H. Vereecken. 2010. Estimating soil hydraulic properties from infrared measurements of soil surface temperatures and TDR data. Vadose Zone J. 9:910–924. doi:10.2136/vzj2009.0176

Sutanto, S.J., J. Wenninger, A.M.J. Coenders-Gerrits, and S. Uhlenbrook. 2012. Partitioning of evaporation into transpiration, soil evaporation and interception: A comparison between isotope measurements and a HYDRUS-1D model. Hydrol. Earth Syst. Sci. 16:2605–2616. doi:10.5194/hess-16-2605-2012

Taylor, S.A., and G.L. Ashcroft. 1972. Physical edaphology: The physics of irrigated and nonirrigated soils. W.H. Freeman, San Francisco.

van Genuchten, M.Th. 1980. A closed-form equation for predicting the hydraulic conductivity of unsaturated soils. Soil Sci. Soc. Am. J. 44:892–898. doi:10.2136/sssaj1980.03615995004400050002x

Van Looy, K., J. Bouma, M. Herbst, J. Koestel, B. Minasny, U. Mishra, et al. 2017. Pedotransfer functions in Earth system science: Challenges and perspectives. Rev. Geophys. 55:1199–1256. doi:10.1002/2017RG000581

Vereecken, H., R. Kasteel, J. Vanderborght, and T. Harter. 2007. Upscaling hydraulic properties and soil water flow processes in heterogeneous soils. Vadose Zone J. 6:1–28. doi:10.2136/vzj2006.0055

Vogel, T., M. Cislerova, and J.W. Hopmans. 1991. Porous media with linearly variable hydraulic properties. Water Resour. Res. 27:2735–2741. doi:10.1029/91WR01676

Vrugt, J.A., and B.A. Robinson. 2007. Improved evolutionary optimization from genetically adaptive multimethod search. Proc. Natl. Acad. Sci. 104:708–711. doi:10.1073/pnas.0610471104

Vrugt, J.A., P.H. Stauffer, T. Wöhling, B.A. Robinson, and V.V. Vesselinov. 2008a. Inverse modeling of subsurface flow and transport properties: A review with new developments. Vadose Zone J. 7:843–864. doi:10.2136/vzj2007.0078

Vrugt, J.A., C.J.F. ter Braak, M.P. Clark, J.M. Hyman, and B.A. Robinson. 2008b. Treatment of input uncertainty in hydrologic modeling: Doing hydrology backward with Markov chain Monte Carlo simulation. Water Resour. Res. 44: W00B09. doi:10.1029/2007WR006720

Wesseling, J., J. Elbers, P. Kabat, and B. Van den Broek. 1991. SWATRE: Instructions for input. Winand Staring Ctr., Wageningen, the Netherlands.

Western, A.W., S.-L. Zhou, R.B. Grayson, T.A. McMahon, G. Blöschl, and D.J. Wilson. 2004. Spatial correlation of soil moisture in small catchments and its relationship to dominant spatial hydrological processes. J. Hydrol. 286:113–134. doi:10.1016/j.jhydrol.2003.09.014

Wöhling, T., and J.A. Vrugt. 2011. Multiresponse multilayer vadose zone model calibration using Markov chain Monte Carlo simulation and field water retention data. Water Resour. Res. 47:W04510. doi:10.1029/2010WR009265

Zreda, M., D. Desilets, T.P.A. Ferré, and R.L. Scott. 2008. Measuring soil moisture content non-invasively at intermediate spatial scale using cosmic-ray neutrons. Geophys. Res. Lett. 35:L21402 doi:10.1029/2008GL035655

Zreda, M., W.J. Shuttleworth, X. Zeng, C. Zweck, D. Desilets, T. Franz, and R. Rosolem. 2012. COSMOS: The cosmic-ray soil moisture observing system. Hydrol. Earth Syst. Sci. 16:4079–4099. doi:10.5194/hess-16-4079-2012